Université de Montréal

«Investigation of the effects of ceramide-C16 and n-decane on the polymorphism of phosphatidylethanolamine; a ^{2}H and ^{31}P solid-state NMR and differential scanning calorimetry study»

Par

Mahmoudreza Doroudgar

Département de chimie, Université de Montréal

Faculté des arts et des sciences

Mémoire présenté à la Faculté des études supérieures et postdoctorales

en vue de l'obtention du grade de maître ès sciences (M.Sc.)

en chimie

Décembre, 2016

Résumé

Les céramides, dont la structure comporte une chaîne hexadecanoyle (CerC16), une chaîne considérée comme de longueur moyenne, sont des sphingolipides impliqués dans de nombreuses pathologies telles que l'obésité, le diabète, la maladie de Parkinson ainsi que certains types de cancer. La première partie de mon projet de M.Sc. a consisté à utiliser la calorimétrie différentielle à balayage (DSC de l'anglais *differential scanning calorimetry*) et la spectroscopie RMN séquentielle à l'état solide du deutérium (^{2}H) et du ^{31}P afin d'étudier l'impact du CerC16 (<20 mol%) sur le polymorphisme de la 1-palmitoyl-2-oléoyl-*sn*-glycéro-3-phosphoéthanolamine (POPE). Les résultats montrent que le CerC16 a un impact majeur. Il élargit la transition de phase lamellaire gel-fluide (L_β–L_α) et la décale vers les hautes températures, ce qui entraîne la création de larges régions de coexistence L_β/L_α dans le diagramme de phase du système. La présence du céramide entraîne également un élargissement de la transition de phase L_α–hexagonale inverse (H_{II}) ainsi qu'une diminution de la température qui lui est associée. Lorsque la proportion de CerC16 dans la membrane de POPE est supérieure à 12-13 mol%, les deux transitions se chevauchent, ce qui entraîne la coexistence des trois phases. Ce chevauchement conduit à une transition de phase directe L_β–H_{II}. De manière générale, le céramide entraîne donc une multitude d'effets sur les propriétés de la membrane lipidique, de la variation de sa fluidité à la modulation de son rayon spontané de courbure.

Certains alcanes de longueurs variables ont le potentiel de favoriser la transition L_α-H_{II} de différentes phosphatidyléthanolamines (PE). Dans la seconde partie de mon M.Sc., j'ai caractérisé les impacts du n-décane-d_{22} (10 mol%), un alcane à courte chaîne, sur le

polymorphisme de la POPE, en exploitant les mêmes techniques de spectroscopie RMN que précédemment. J'ai montré que, malgré une diminution significative de la température associée au début de transition L_α–H_{II}, la température de la fin de transition restait quant à elle sensiblement inchangée. Globalement, la transition est donc élargie. Nous proposons que les molécules de n-décane se localisent au niveau des bouts de chaînes acyles de la POPE en phase L_α, ce qui engendre des compressions et des contraintes. Il en résulte un décalage du début de transition L_α–H_{II} vers les basses températures. Lorsque la température augmente, de plus en plus de molécules de n-décane sont transférées vers la phase H_{II}, ce qui réduit les contraintes sur les chaînes acyles de la phase L_α. Le décane comble les espaces entre les cylindres H_{II} et favorise aussi de cette manière la phase non-lamellaire.

Mots clés : polymorphisme, gel, liquide cristalline, hexagonale inversée, diagramme de phase.

Abstract

Ceramide C16 (CerC16), a mid-chain sphingolipid bearing a hexadecanoyl chain, is involved in several diseases such as diabetes, obesity, Parkinson, and certain type of cancers. In the first part of my M.Sc. project, I employed differential scanning calorimetry (DSC) and sequential ^{2}H and ^{31}P static solid-state NMR spectroscopy to study the role of CerC16 ($\leq$ 20 mol%) in modifying the polymorphism of 1-palmitoyl-2-oleoyl-*sn*-glycero-3-phosphoethanolamine (POPE). The results demonstrate that CerC16 has major impacts. It broadens the gel–fluid lamellar (L_β–L_α) phase transition and shifts it toward higher temperatures. This effect leads to the creation of a wide L_β/L_α coexistence region in the phase diagram of the system. CerC16 also broadens the L_α–inverted hexagonal (H_{II}) phase transition and shifts it towards lower temperatures. When CerC16 proportion in POPE bilayers is $\geq$ 12-13 mol%, the two transitions overlap, leading to a three-phase coexistence line in the phase diagram. Such a phenomenon leads to a direct L_β–H_{II} phase transition. Globally, CerC16 can have a wide range of effects on membrane properties, from varying its fluidity to modulating its curvature.

Alkanes of various chain lengths are able to promote the L_α–H_{II} transition of different phosphatidylethanolamines (PE). In the second part of my M.Sc. thesis, I investigated the impacts of 10 mol% n-decane-d_{22}, a short alkane, on the polymorphism of POPE, using sequential ^{2}H and ^{31}P solid-state NMR spectroscopy. The results show that although, n-decane causes a significant downshift in the onset temperature of the L_α–H_{II} transition, it does not shift considerably the end of the transition. As a consequence, a very broad L_α–H_{II} transition is obtained. It is inferred that n-decane molecules are found within the lower part of the POPE acyl chains in the L_α phase. This

location increases the chain packing stress and consequently, initiates the L_{α}–H_{II} transition at lower temperatures. Upon increasing temperature, more and more n-decane molecules are transferred to the H_{II} phase; the relocation not only decreases the chain packing stress in the L_{α} phase, but also allows the decane molecules to fill the interstitial void spaces between the H_{II} cylinders.

Keywords: polymorphism, gel, liquid crystalline, inverted hexagonal, phase diagram.

Contents

Table

Figures

Abbreviations

AFM: atomic force microscopy

B_0: external magnetic field

Bax protein: bcl-2-like protein 4

CerC16: N-palmitoyl-D-erythro-sphingosine

CerC16-d_{31}: N-palmitoyl-d_{31}-D-erythro-sphingosine

CSA: chemical shift anisotropy

DAG: diacylglycerol

δ_{ISO}: isotropic phase chemical shift tensor

$\delta_{\parallel}$: parallel averaged chemical shift tensor

$\delta_{\perp}$: perpendicular averaged chemical shift tensor

DEPE: 1,2-dierucoyl-sn-glycero-3-phosphoethanolamine

DiIC18: 1,1'-dioctadecyl-3,3,3',3'-tetramethylindocarbocyanine perchlorate

DMPC: 1,2-dimyristoyl-*sn*-glycero-3-phosphocholine

DOPE: 1,2-dioleoyl-sn-glycero-3-phosphoethanolamine

DPPC: 1,2-dipalmitoyl-*sn*-glycero-3-phosphocholine

DSC: differential scanning calorimetry

EDTA: ethylenediaminetetraacetic acid

EFG: electric field gradient

η: asymmetry parameter

H_I: hexagonal phase

H_{II}: inverted hexagonal phase

HEPES: 4-(2-hydroxyethyl)piperazine-1-ethanesulfonic acid

HPLC: high performance liquid chromatography

I: nucleus spin number

L_α: liquid crystalline phase

L_β: gel phase

m_I: nucleus spin quantum number

NMR: nuclear magnetic resonance

ω_Q: quadrupolar coupling constant

π: pressure integral

PC: phosphatidylcholine

PE: phosphatidylethanolamine

POPC: 1-palmitoyl-2-oleoyl-*sn*-glycero-3-phosphocholine

POPE: 1-palmitoyl-2-oleoyl-*sn*-glycero-3-phosphoethanolamine

POPE-d_{31}: 1-palmitoyl-d_{31}-2-oleoyl-sn-glycero-3-phosphoethanolamine

PS: phospho-L-serine

PSM: N-palmitoyl-sphingomyelin

Q: nuclear electric quadrupole moment

Q_{II}: inverted micellar cubic phase

R_0: intrinsic radius of curvature

RBC: red blood cell

RF: radio frequency

RMN: résonance magnétique nucléaire

T: torque

T_H: fluid-to-inverted hexagonal transition temperature

T_m: gel-to-fluid transition temperature

SC: spontaneous curvature

Appreciations

I would like to express my sincere appreciation to my supervisor Prof. Michel Lafleur for providing me with the great opportunity to perform esearch in the domain of biophysics, and for generously offering his precious time to keep my M.Sc. project always on the right path.

I would also thank my colleagues, Adrian and Mehdi, who helped me a lot to settle in the group and quickly start my researches in the lab. I also thank the National Sciences and Engineering Research Council of Canada, NSERC, for financially supporting my M.Sc. project.

تقدیم به پدر و مادرم

Chapter 1: Introduction

1.1 How do some lipid bilayers adopt non-bilayer morphologies?

The ability of lipids to self-assemble into dynamic microstructures is of central importance since living cells are highly dependent on the proper functioning of self-assembled microstructures such as their plasma membrane (Fig. 1.1). In water, lipid molecules gather together to form self-assembled microstructures because the head group and the acyl chains have different polarities. In fact, they arrange themselves in a way, so that the polar (hydrophilic) head groups are in contact with polar water molecules, and the apolar (hydrophobic) acyl chains are shielded in the middle of the aggregate, away from the water medium. Depending on some specific factors, lipid molecules can self-assemble into a variety of morphologies (different phases), such as gel (L_β), liquid crystalline (L_α), or inverted hexagonal (H_{II}) (Fig. 1.2); this phenomenon is called "polymorphism". The factors influencing the morphology of the self-assembled structures could be related to molecular features such as the bulkiness of the polar head group and the length of the apolar acyl chain, as well as external conditions such as temperature, pH, etc. The variations of these factors may cause the conversion of one phase to another, i.e. a phase transition.

Cellular membranes have a highly dynamic behavior as they are in constant interactions with other cells, as well as the surrounding medium. They not only have to preserve their lamellar morphology at large scale, but also need to maintain their molecular dynamics at smaller scales (1, 2). To obtain a balance between the stability and dynamics of their membranes, living cells employ a combination of lipid species. As a comparison between different lipid species,

phosphatidylcholine (PC) forms stable lipid bilayers under physiological conditions. Conversely phosphatidylethanolamine (PE) and diacylglycerol (DAG) can exhibit both bilayer and non-bilayer structures under different conditions. As a consequence, their presence in PC bilayers can destabilize the lamellar structure (3). The presence of lipids capable of forming non-bilayer structures is essential in the proper functioning of cell membranes. For instance, they can mediate protein–lipid interactions and modulate protein activity (4).

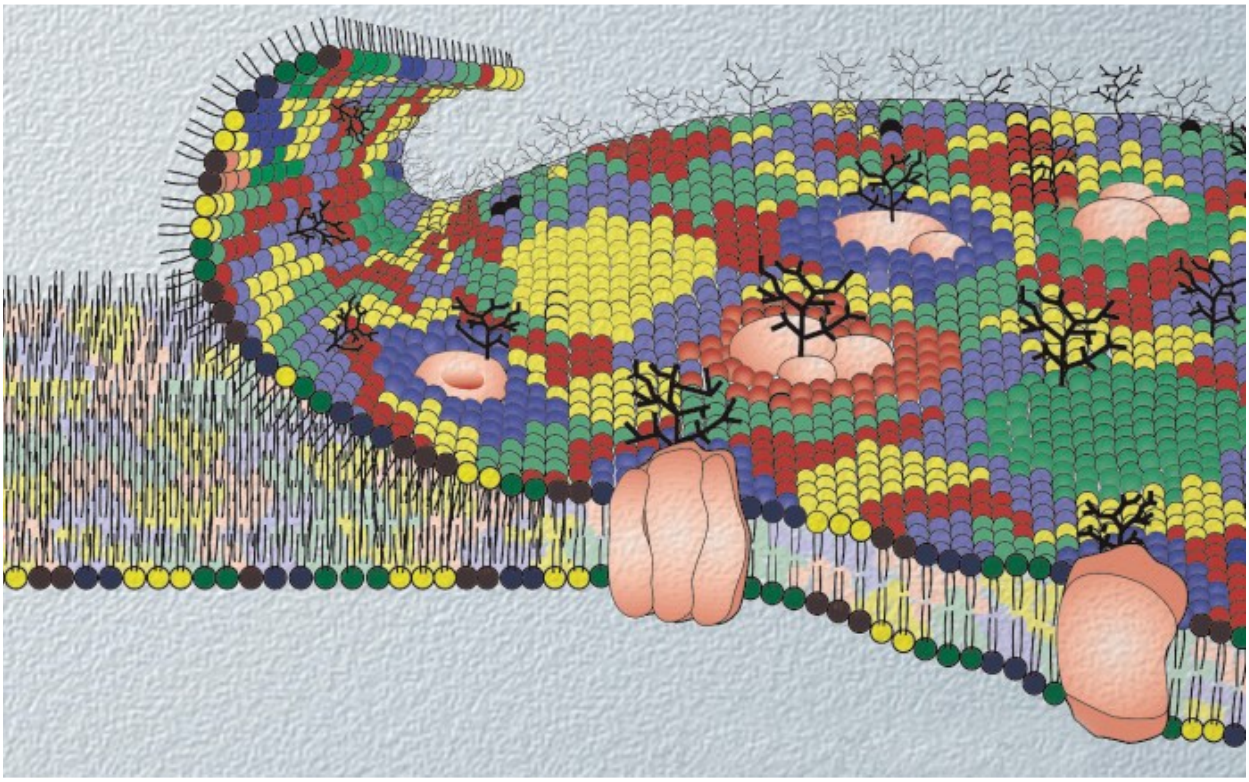

Fig. 1.1: A schematic of the eukaryotic plasma membrane. The various phospholipid species are shown in different colors. The figure was reproduced by permission from the Nature Reviews Molecular Cell Biology (5).

Non-bilayer lipids can also modulate the local curvature of lipid bilayers (6). As an indication of their important role, one can imply to some microorganisms that alter the ratio between their bilayer and non-bilayer forming lipids as a function of the environment temperature (7). Besides the dynamic regulation of the bulk lipid composition, cell membranes display asymmetric lipid distribution between the two monolayers. For instance, in plasma membranes, PE and phospho-L-serine (PS), are accumulated within the monolayer in contact with the cytoplasm (6, 8).

Considering a relaxed lipid bilayer at equilibrium, the balance of all the lateral forces, both attractive and repulsive, applied on the different parts of either of the monolayers must set the pressure integral on the bilayer (π) to zero (Fig. 1.3). A lipid monolayer is formed of three different parts: the head groups, the acyl chains, and the head group/acyl chain interface. The later has a very critical role since any increase in this area is energetically costly, and leads to an exposure of the acyl chains to water. The head groups can be affected by environment conditions and a change in their structure can result in perturbing the pressure profile and consequently, the stability of the lipid bilayer. Globally, an uneven distribution of the positive and negative forces applied across the different parts of a lipid bilayer leads to a nonzero integral torque (*T*) that can bend the monolayers in opposite directions. As a comparison, the entropic repulsion is more significant in the lipid bilayers consisted of lipids with bulky acyl chains. The strong entropic force then powerfully pushes the acyl chains apart resulting either the lipid monolayers to acquire higher degrees of curvature and eventually be separated. However, this monolayers separation is unfavorable from a thermodynamic point of view as it would create voids inside the membrane (9).

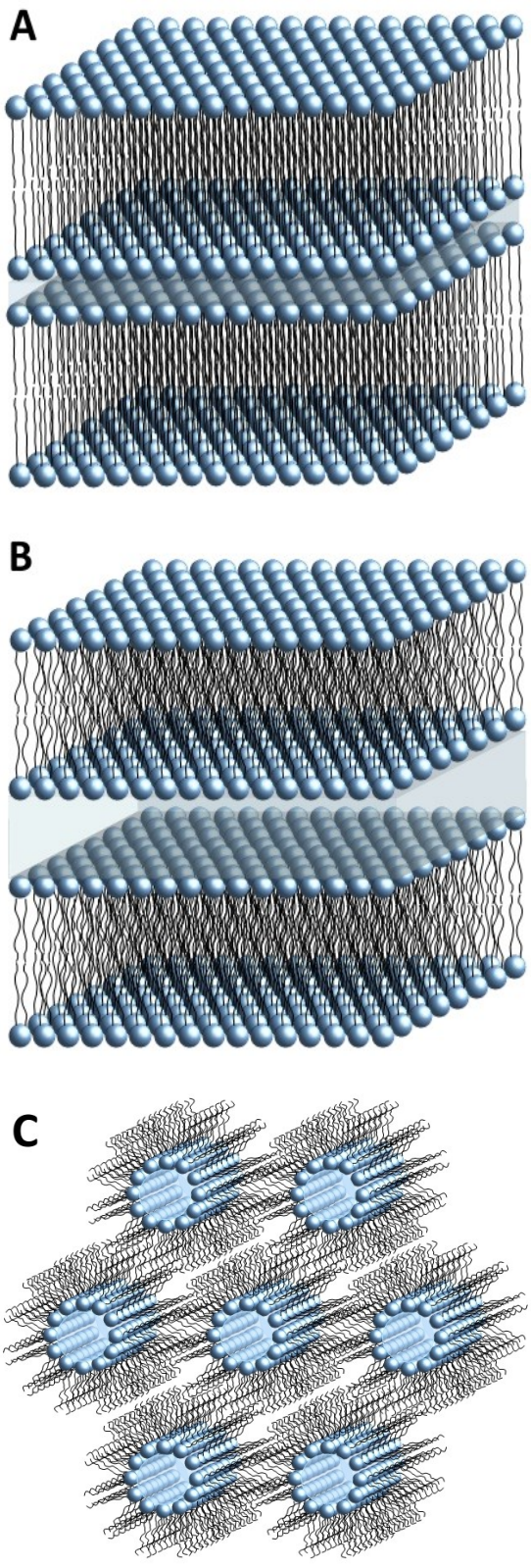

Fig. 1.2: Schematics of (A) gel (L_β), (B) liquid crystalline (L_α), and (C) inverted hexagonal (H_{II}) phases.

Therefore, the unbalance torque results in the creation of an "elastic stress" stored in the bilayer. This stress could be accumulated until a critical value that is intrinsic for a given bilayer and correlated with the shape of the constituent lipids (10). If the accumulated elastic stress exceeds the critical value, the two monolayers separate apart, forming non-bilayer phases such as hexagonal (H_I), inverted hexagonal (H_{II}), inverted micellar cubic (Q_{II}), etc. For example, it was shown that CerC16, a sphingolipid bearing a small head group and used in the present work, induce a decrease in the L_α–H_{II} transition temperature of 1,2-dierucoyl-sn-glycero-3-phosphoethanolamine (DEPE) (11).

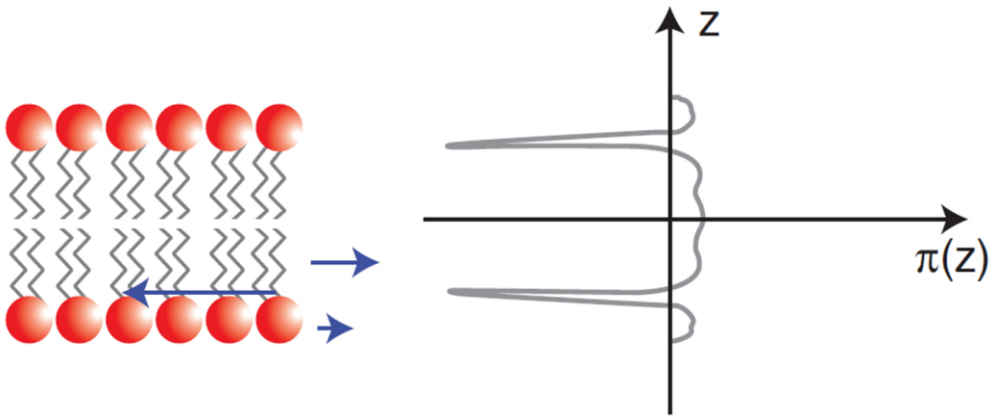

Fig. 1.3: A schematic of the pressure profile (π) due to the lateral forces (blue arrows) applied across the different parts of a relax bilayer at equilibrium. The figure was reproduced by permission from the Cold Spring Harbor Perspectives in Biology Journal (10).

Another model that rationalizes the different phase behavior of various lipids is based on the intrinsic molecular morphology of each lipid. The shape of a lipid molecule can be characterized by a packing parameter, P, defined as $P = V/al$ where V is the specific volume occupied by the acyl chains, a is the area per lipid molecule at the polar/apolar interface, and l

is the effective length of the acyl chains (12). The P parameter describes the effective shape of the lipid molecule in fluid state: $P \approx 1$ for cylinder shape molecule such as 1-palmitoyl-2-oleoyl-sn-glycero-3-phosphocholine (POPC), $P > 1$ for cone shape lipids such as 1-palmitoyl-2-oleoyl-sn-glycero-3-phosphoethanolamine (POPE), and $P < 1$ for inverse cone shape lipids such as lysophosphocholine (LPC) (Fig. 1.4). In fact, one could make a bridge between the two abovementioned models – torque model and intrinsic molecular morphology model, as P defines the spontaneous curvature (SC) of a lipid monolayer (13); SC is obtained when the torque applied across the lipid monolayer is zero, and thus, the curvature of the lipid monolayer is imposed by the morphology of the constituent lipid molecules. It should be noted that in case of the multicomponent monolayers, the curvature is approximately the average of those of all the lipid constituents (14). Monolayers constructed by cylindrical lipid molecules ($P \approx 1$) form bilayers under zero SC condition. However, lipids with $P \neq 1$ inserted in bilayers have to "reshape" into cylindrical morphologies. This lipids reconfiguration into cylindrical morphologies causes stress on the bilayers as V, the acyl chain volume of the lipids, must remain constant, and thus, the acyl chains have to be either stretched or squeezed.

Globally, the *P* value illustrates how far a bilayer curvature diverges from the SC, or in other words, how strong the stored stress propels the bilayer toward non-bilayer morphologies. The transformation of lipid bilayer to non-bilayer morphologies is a typical example of lipid polymorphism (7). It should be noted that different lipid molecules with $P > 1$, could make "inversed" non-bilayer phases of various morphologies such as H_{II}, Q_{II}, etc. As an example, one could mention about the hexagonal (H_I) and inversed hexagonal (H_{II}) phases in which the monolayers fit into closely packed cylindrical structures. The only difference between these two

phases is the orientation of the molecules relative to the cylinders. In the H_I phase, the acyl chains are toward the center of the cylinders while they point away from the cylinder center in the H_{II} phase, the middle of the cylinder being filled with water.

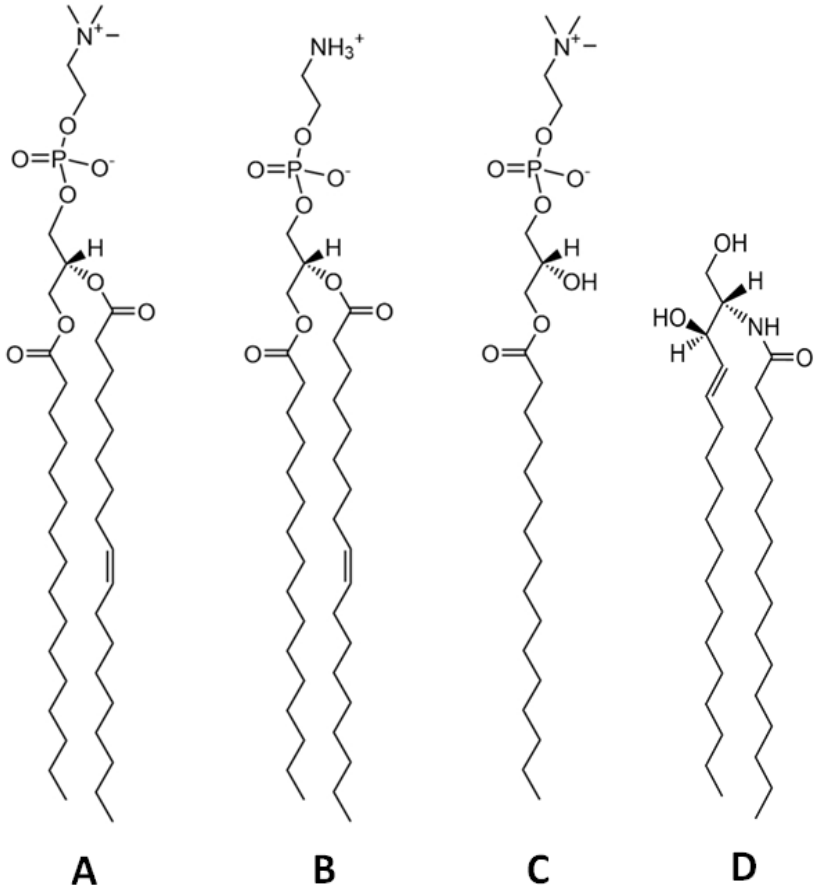

Fig. 1.4: The structure and main phase transition temperature of **(A)** POPC, T_m = -2.6 ^oC (15), **(B)** POPE, T_m = 25 ^oC, **(C)** 16:0 LPC, T_m = 3.4 ^oC (16), and **(D)** CerC16, T_m = 91 ^oC (17).

1.2 Brief introduction to the project

My M.Sc. project is focused on two main aspects:

- Ceramide-C16 as a versatile modulator of phosphatidylethanolamine polymorphism,
- Characterization of n-decane distribution within phosphatidylethanolamine L_α/H_{II} phases.

1.2.1 Ceramide-C16 is a versatile modulator of phosphatidylethanolamine polymorphism

As the first part of the project, I studied the effects of CerC16, an important sphingolipid involved in several diseases such as diabetes, obesity, Parkinson, etc., on the polymorphism of POPE membrane. It has been reported that CerC16 exhibits a L_β–L_α transition at ~91 ^oC (17), while POPE goes through two phase transitions: a L_β–L_α phase transition at ~25 ^oC (18), and a L_α–H_{II} phase transition at ~71 oC (19). The findings are presented in chapter 2; it corresponds to a publication accepted by *Biophysical Journal*. I employed DSC for measuring the thermal behavior of both pure POPE and POPE/CerC16 dispersions of various molar fractions. I also used sequentially ^2H and ^{31}P-NMR spectroscopy for calculating the phase distribution, as well as measuring the acyl chains dynamic of either the components – POPE and CerC16, within various phases at different temperatures.

1.2.2 Characterization of n-decane distribution within phosphatidylethanolamine L_α/H_{II} phases

As the second part of the project, I studied how n-decane, a simple aliphatic chain, is distributed in the L_α/H_{II} phases of POPE. The promotion of H_{II} phase of POPE by n-decane was also investigated. Similar to the first part of the project, sequential ^{2}H and ^{31}P solid-state NMR spectroscopy at different temperatures was employed for measuring the phase distribution of both components – POPE and n-decane, within either the phases at different temperatures.

1.3 Techniques

1.3.1 Differential scanning calorimetry (DSC)

In DSC the amount of energy absorbed or released by a sample is measured with respect to that of a reference, providing quantitative and qualitative data on endothermic (heat absorption) and exothermic (heat evolution) processes. Technically, a differential method is applied to continuously measuring the heat flow into the sample, and equalizing the implicit heat gains and losses between the sample and the reference (20). Since heat flow is measured under constant pressure in DSC, the variation of heat flow into the sample is equivalent to enthalpy changes, $\left(\frac{dq}{dt}\right)_P = \frac{dH}{dt}$. The Heat capacity of the sample, C_P, is determined as:

$$C_P = \Delta\left(\frac{dH}{dT}\right)_P \qquad \textbf{Eq.}\ 1.1$$

By rearranging Eq. 1.1 as,

$$C_P = \Delta\left(\frac{dH}{dT}\right)_P = \Delta\frac{dH}{dt}\frac{dt}{dT} = \Delta\left(\frac{dq}{dt}\right)_P\frac{dt}{dT}$$ **Eq.** 1.2

where $\left(\frac{dq}{dt}\right)_P$ is the variation of the heat flow into the sample and $\frac{dt}{dT}$ is the inverse of the temperature scan rate, one can plot the changes in the heat capacity of the sample versus temperature – C_P thermogram. Finally, one can calculate the total enthalpy of a phase transition of the sample by integrating the area under the peak of the obtained C_P thermogram as,

$$\Delta H = \int_{T_1}^{T_2} C_P dT$$ **Eq.** 1.3

(Fig. 1.5). The thermograms of a lipid mixture, generally much broader than those of its pure lipid constituents, that allows determining the phase coexistence regions.

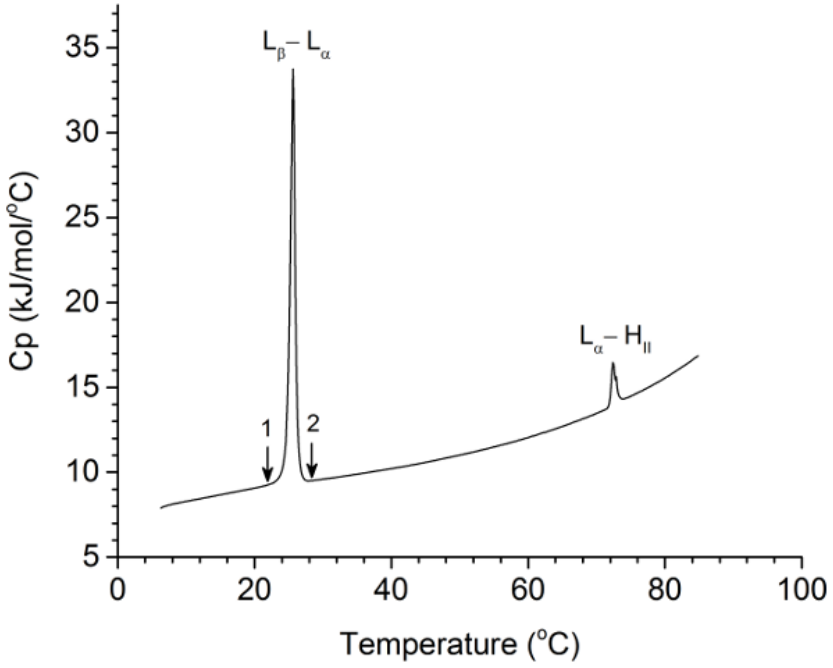

Fig. 1.5: The concentration normalized heat capacity thermogram of a pure POPE dispersion. Noted that the arrows presented on the thermogram indicate the beginning, 1, and the end, 2, of the L_β–L_α transition of the POPE dispersion used in measuring the integral of the thermal peak.

1.3.2 Solid state nuclear magnetic resonance

Solid state nuclear magnetic resonance (NMR) spectroscopy is a useful technique commonly exploited in a wide range of applications, from characterizing the synthetic products to studying the molecular structure of some complex systems such as catalysts, polymers, and proteins. In a solid compound, molecules do not move as freely as they do in liquids.

The nucleus spin number (I) is the main parameter that defines the kind of coupling interaction that various nuclei go through with the external magnetic field. As a global classification based on I, different nuclei can be categorized into two groups of $I = 1/2$ such as ^{1}H and ^{31}P, and $I > 1/2$ (quadrupolar nuclei) such as ^{2}H. Overall, there are $2I + 1$ energy levels characterized by the nucleus spin quantum number (m_I). While nuclei of $I = 1/2$ divided to two energy levels [$m_l = +1/2, -1/2$], there are three [$m_l = +1, 0, -1$] for the nuclei of $I = 1$. Nuclei of $I > 1/2$ possess non-spherical charge distributions. The charge asymmetry of the quadrupolar nuclei can couple with electric-field gradients, EFG. This phenomenon is responsible for the so-called "quadrupolar splitting" seen in the solid-state NMR spectra of the $I > 1/2$ nuclei. In this project, I have performed static solid-state NMR of phosphorus (^{31}P, $I = 1/2$), this nucleus being present in the polar head group of POPE, and of deuterium (^{2}H, $I = 1$), using perdeuterated acyl chains of either N-palmitoyl-D-erythro-sphingosine (CerC16-d_{31}) or POPE-d_{31} or n-decane-d_{22}. The phenomena leading to the peak broadening, namely, chemical-shift anisotropy (CSA) and quadrupolar splitting, are presented in the next section.

1.3.2.1 Chemical-shift anisotropy (CSA)

The CSA is one of the factors that has major influences on defining the broadness and shape of the ^{31}P powder pattern in the solid-state NMR spectroscopy. The origin of CSA can be explained considering the fact that the electron cloud around such nucleus does not display a spherical shape. Since the electron density affects the resonance frequency of a nucleus (the chemical shift), the orientation of the electron cloud, and thus, the orientation of the molecule with respect to B_0 defines the resonance frequency of a nucleus in a solid sample. The CSA of a $I = 1/2$ nucleus is representative of the asymmetric electron distribution around the nucleus (Fig. 1.6A). The chemical shift anisotropy can be represented by a diagonalized tensor – a 3×3 matrix with non-zero elements only on the diagonal. The highest and lowest chemical shifts are referred as δ_{11} and δ_{33} – the first and third principal axis, respectively. The chemical shift value of δ_{22} – the one between δ_{11} and δ_{33}, is perpendicular to both δ_{11} and δ_{33}. Since numerous crystalline regions of random orientations are found in powders, the signal superposition of such crystalline regions defines a spectrum line shape schematically represented in Fig. 1.6B.

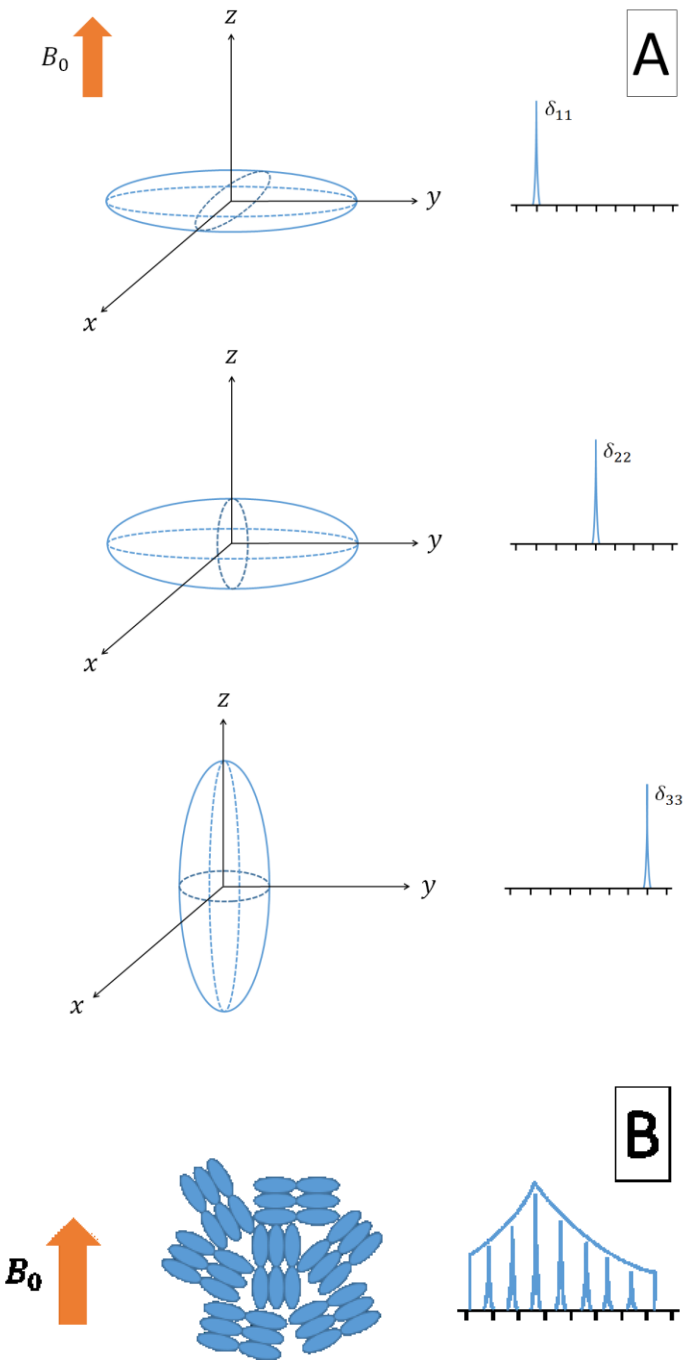

Fig. 1.6: (A) A schematic representation of the orientation effect of the ellipsoidal CSA principal values of a single nucleus of $I = 1/2$. (B) The effect of random orientation of various crystalline regions leading to a powder pattern line shape.

As mentioned earlier, lipid molecules experience various motion restrictions in different phases. In the case of L_β phase, the motions are highly restricted, giving rise to a wide powder pattern because of the limited averaging of the CSA. In L_α phase, the lipid molecules rotate fast (on the NMR time scale) around their main molecular axis. This rotation results in averaging the chemical shift tensor that is reduced to 2 components: $\delta_{\parallel}$, the parallel component and $\delta_{\perp}$, the perpendicular component with respect to the symmetry axis of the molecules. For liposomes in the L_α phase, a powder pattern typical of axial symmetry is obtained (Fig. 1.7; top). In the case of the H_{II} phase, lipid molecules experience a second fast rotation: their diffusion around the main axis of symmetry of the H_{II} phase cylinders. This additional motion results in further averaging of the chemical shift tensors and reduces the CSA by a factor -1/2 compared to that of the L_α phase (Fig. 1.7B). In some lipid phases, such as inverted micellar cubic (Q_{II}), there could be isotropic motions causing complete averaging of the CSA; a very narrow peak similar to those of liquid samples appeared at δ_{ISO}.

The ^{31}P solid-state NMR signal of phospholipids could also be broadened because of ^{31}P–^{1}H coupling interaction as several ^{1}H nuclei exist around the phosphorus nucleus. To eliminate this coupling, one needs to use a ^{1}H decoupling technique. Although, there are various techniques that could be utilized to decouple ^{1}H–^{31}P interactions, they are all based on the introduction of a radio frequency (RF) pulse at the ^{1}H frequency. In this project, I used a low-power decoupling method so-called “Waltz65”. The reason I chose a low-power decoupling technique was to avoid thermal perturbation of the sample.

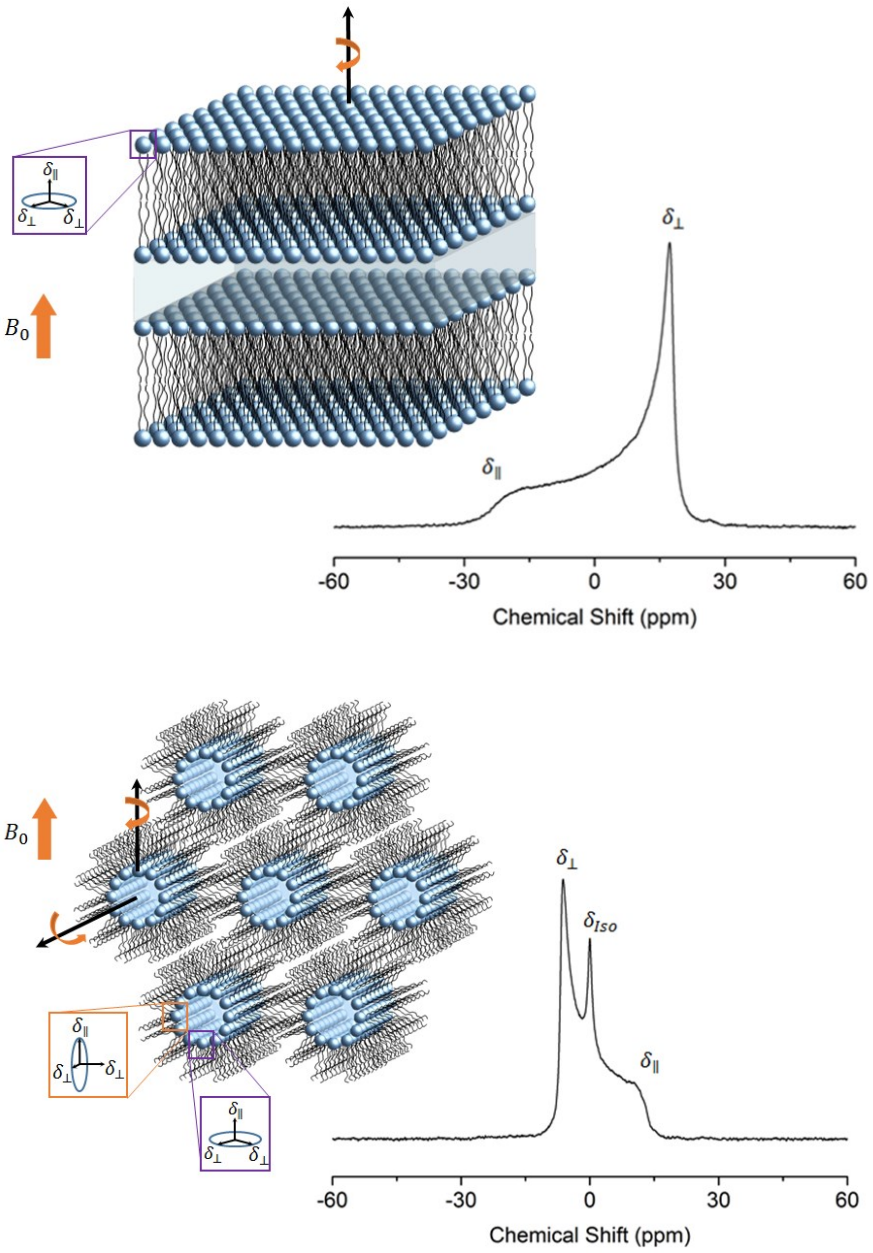

Fig. 1.7: ^{31}P-NMR spectra of (top) lamellar (L_α), and (bottom) inverted hexagonal (H_{II}) phases of POPE. The averaged chemical shift tensors, $\delta_\perp$ and $\delta_\parallel$, are schematically presented for each phases.

1.3.2.2 Quadrupolar splitting

Regardless of its poor abundance, but because of the valuable information that could be obtained from, deuterium (^{2}H, $I = 1$) has been one of the most studied quadrupolar nuclei in all fields (21, 22). Since ^{2}H has a small electron cloud and a fairly low gyromagnetic ratio ($\sim 1/7$ of ^{1}H), this nucleus displays a small chemical shift of ~3–4 ppm. However, ^{2}H spectrum of a solid sample could be as wide as ~100 kHz. The origin of the ^{2}H spectrum broadness is the quadrupolar interactions. As mentioned earlier, nuclei of $I = 1$ such as ^{2}H display three energy levels, $[+1, 0, -1]$. Once placed in an external magnetic field, ^{2}H nuclei are allowed to perform two transitions: $+1 \rightarrow 0$ and $0 \rightarrow -1$. Taking in into account only the Zeeman interaction, the two transitions should involve the same amount of energy, i.e. they should occur at the same frequency. However, the quadrupolar interactions disturb the Zeeman energy levels, so the energy differences associated with the two transitions are no longer equal. The strength of these interactions is described by the quadrupolar coupling constant, ω_Q, which is relative to Q, the nuclear electric quadrupole moment of the nucleus (Fig. 1.8A). Q defines how strong a quadrupolar nucleus interacts with the electric field gradient. Because ^{2}H has a relatively small Q value ($3 \times 10^{-31}\ m^2$), its ω_Q is around 100–300 kHz (23); as a comparison, ω_Q of ^{14}N is ≥ 3 MHz (24).

The powder pattern of quadrupolar nuclei, depends on the asymmetry parameter, $\eta = \frac{V_{xx} - V_{yy}}{V_{zz}}$ where V_{xx}, V_{yy}, V_{zz} are the principal components of the electric field gradient around the nucleus. Similar to CSA, the first-order quadrupolar coupling is dependent on the orientation of the molecules with respect to B_0.

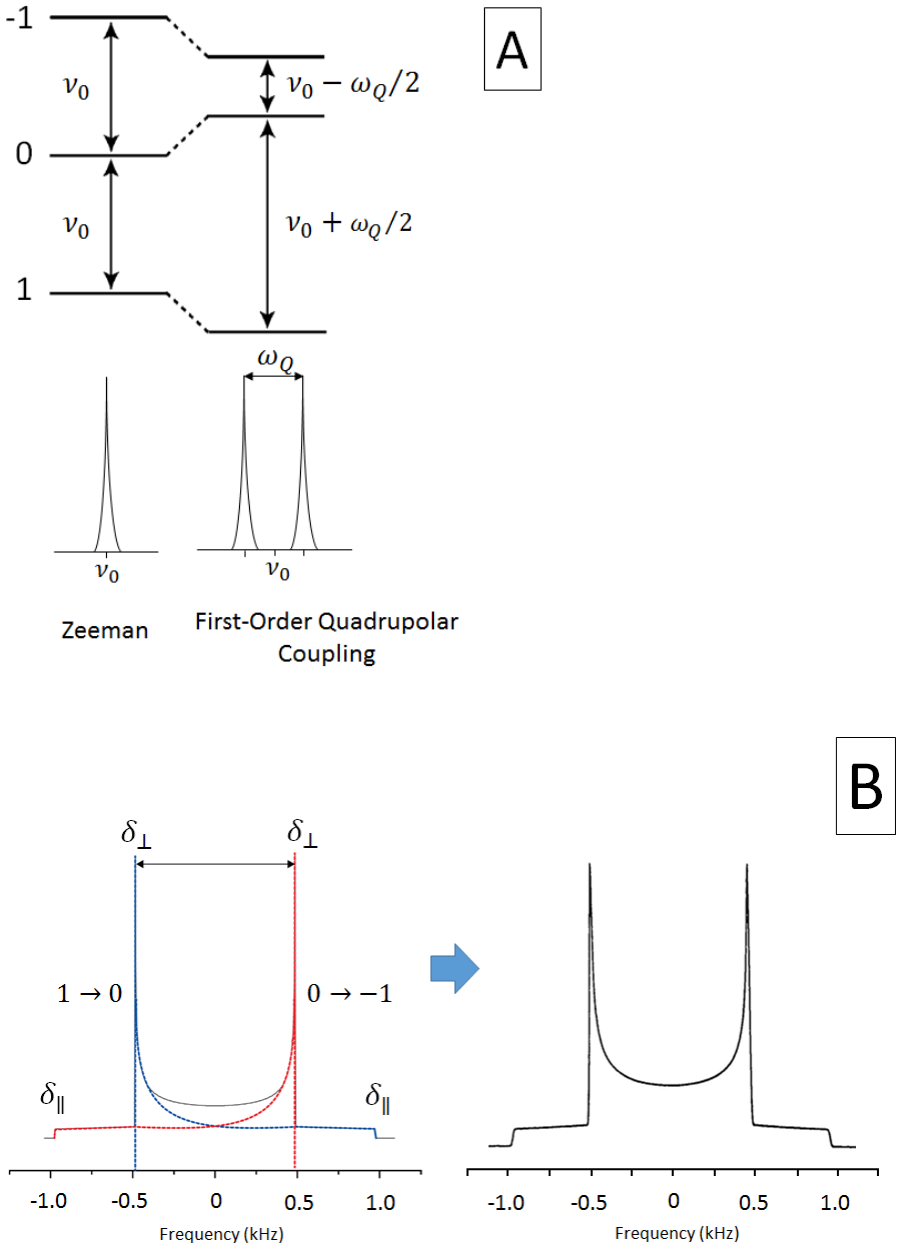

Fig. 1.8: (A) A schematic representation of the disturbance effect of the first-order quadrupolar coupling on the two equal Zeeman transitions of the $I = 1$ nuclei of a single crystal. (B) A ^{2}H quadrupolar coupling powder pattern when the asymmetry parameter, η, is zero.

The carbon-deuterium bonds found on a perdeuterated lipid acyl chain display an electric field gradient that has a cylindrical symmetry, with an axis of symmetric along the C-D bond. Therefore V_{xx} is equal to V_{yy}, which makes η become zero. Once $\eta = 0$, the quadrupolar coupling of ^{2}H nuclei is defined as $\upsilon_Q = \frac{3}{4}\frac{e^2qQ}{h}(3cos^2\theta - 1)$, where e, q, Q, and h are the electron charge, the nucleus charge, the nucleus electric quadrupole moment, and the Planck constant, respectively. Therefore, υ_Q displays an orientational dependency to θ, the angle between V_{zz} and B_0. Therefore, the resulting powder pattern is represented by a "double-horn" spectrum as shown in Fig. 1.8B.

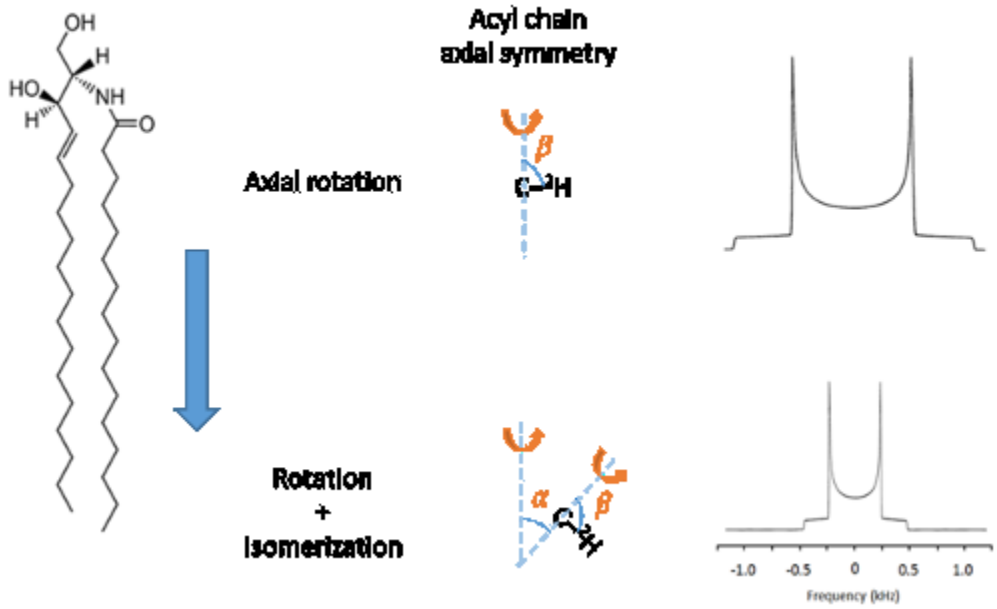

Fig. 1.9: A schematic representation of the effect of different C–^{2}H motions along a lipid acyl chain on the powder patterns.

It should be noted that various C–^{2}H bonds along to a lipid acyl chain display different motions dependent on how far they are positioned from the polar head group (Fig. 1.9). In other words, the level of restriction applied on different C–^{2}H bonds along to the lipid acyl chain varies with the most for those close to the head group to the least for the terminal methyl. This variation in the level of motion demonstrated by different C–^{2}H bonds produces a series of superimposed powder patterns which are more visually resolved in the case of a L_α phase spectrum (Fig. 1.10B). The other aspect that has significant impact on the powder patterns of a deuterated lipid acyl chain is the different motions that lipid molecules experience in various phases. As an example, lipids in an L_β phase rotate slowly on the NMR time scale, leading to a very broad, almost featureless spectrum. The same molecules experience much less restriction in the L_α phase as they rotate rapidly around their principal axis of symmetry. In H_{II} phase, the lipids experience a fast diffusion around the H_{II} cylinders' axes of symmetry, reducing the width of the spectrum by a factor of $\sim$2 compared to that of the L_α phase (Fig. 1.10, bottom) due to an extra averaging of θ. Globally, the static ^{2}H NMR spectrum acquisition is an advantageous technique, as it allows a phase identification, provides information on internal molecular motions (21, 25), and characterize internal molecular orientations and orders (26, 27).

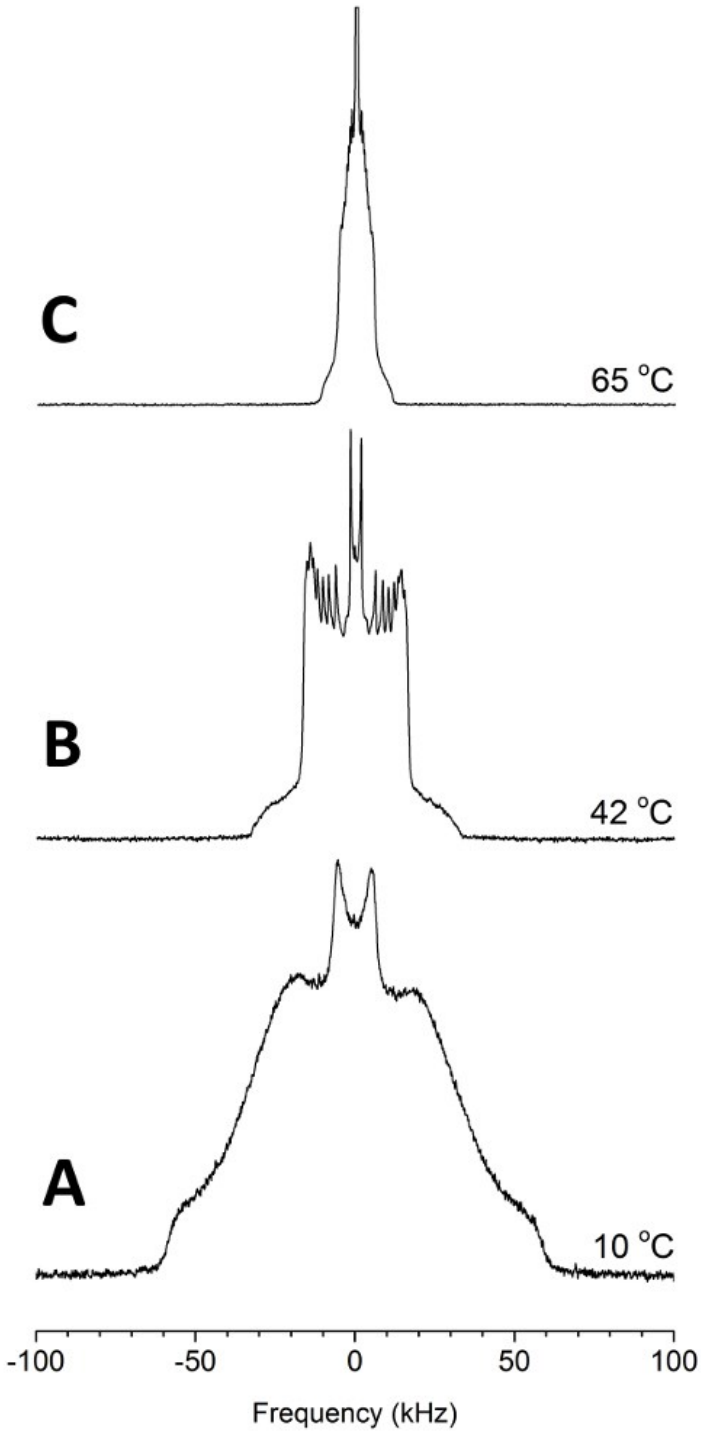

Fig. 1.10: The ^{2}H-NMR spectra of L_{β} (A), L_{α} (B), and H_{II} (C) phases of a POPE-d^{31}/CerC16 90/10 mol% dispersion.

1.4 References

1. McMahon, H. T., and J. L. Gallop. 2005. Membrane curvature and mechanisms of dynamic cell membrane remodelling. *Nature* 438:590–596.
2. Paiement, J., and J. Bergeron. 2001. The shape of things to come: Regulation of shape changes in endoplasmic reticulum. *Biochem. Cell Biol.* 79:587–592.
3. Cullis, P. R., and B. De Kruijff. 1979. Lipid polymorphism and the functional roles of lipids in biological membranes. *Biochim. Biophys. Acta* 559:399–420.
4. Lee, A. G. 2004. How lipids affect the activities of integral membrane proteins. *Biochim. Biophys. Acta* 1666:62–87.
5. Edidin, M. 2003. Lipids on the frontier: A century of cell-membrane bilayers. *Nat. Rev. Mol. Cell Biol.* 4:414–418.
6. Hafez, I. M., and P. R. Cullis. 2001. Roles of lipid polymorphism in intracellular delivery. *Adv. Drug Del. Rev.* 47:139–148.
7. de Kruijff, B. 1997. Lipid polymorphism and biomembrane function. *Curr. Opin. Chem. Biol.* 1:564–569.
8. van Meer, G., D. R. Voelker, and G. W. Feigenson. 2008. Membrane lipids: Where they are and how they behave. *Nat. Rev. Mol. Cell Biol.* 9:112–124.
9. Gruner, S. M. 1989. Stability of lyotropic phases with curved interfaces. *J. Phys. Chem.* 93:7562–7570.
10. Frolov, V. A., A. V. Shnyrova, and J. Zimmerberg. 2011. Lipid polymorphisms and membrane shape. *Cold Spring Harb. Perspect. Biol.* 3:a004747.
11. Sot, J., F. J. Aranda, . . ., and A. Alonso. 2005. Different effects of long- and short-chain ceramides on the gel-fluid and lamellar-hexagonal transitions of phospholipids: A calorimetric, NMR, and X-ray diffraction study. *Biophys. J.* 88:3368–3380.
12. Israelachvili, J. 1992. *Intermolecular and surface forces*. Academic, Santa Barbara, CA.
13. Gruner, S. M. 1985. Intrinsic curvature hypothesis for biomembrane lipid composition: A role for nonbilayer lipids. *Proc. Natl. Acad. Sci.* 82:3665–3669.
14. Kumar, V. V. 1991. Complementary molecular shapes and additivity of the packing parameter of lipids. *Proc. Natl. Acad. Sci. USA* 88:444–448.
15. Keough, K. M. W. 1986. Modifications of lipid structure and their influence on mesomorphism in model membranes: The influence of hydrocarbon chains. *Biochem. Cell Biol.* 64:44–49.
16. Klopfenstein, W. E., B. de Kruyff, . . ., and L. L. M. van Deenen. 1974. Differential scanning calorimetry on mixtures of lecithin, lysolecithin and cholesterol. *Chem. Phys. Lipids* 13:215–222.
17. Shah, J., J. M. Atienza, . . ., and G. G. Shipley. 1995. Structural and thermotropic properties of synthetic C16:0 (palmitoyl) ceramide: Effect of hydration. *J. Lipid Res.* 36:1936–1944.
18. Pozo Navas, B., K. Lohner, . . ., and G. Pabst. 2005. Composition dependence of vesicle morphology and mixing properties in a bacterial model membrane system. *Biochim. Biophys. Acta* 1716:40–48.
19. Silvius, J. R. 1982. *Thermotropic phase transitions of pure lipids in model membranes and their modifications by membrane proteins.* In Lipid-protein interactions. John Wiley & Sons, Inc., New York.
20. Wunderlich, B. 2005. *Thermal analysis of polymeric materials.* Springer-Verlag Berlin Heidelberg, Netherlands.
21. Jelinski, L. W. 1985. Solid state deuterium NMR studies of polymer chain dynamics. *Annu. Rev. Mater. Sci.* 15:359–377.

22. Fluck, E., N. Chandrakumar, and H. Günther. 1996. *Spin-1 NMR.* Springer Berlin Heidelberg, Berlin, Germany.
23. Mantsch, H. H., H. Saitô, and I. C. Smith. 1977. Deuterium magnetic resonance, applications in chemistry, physics and biology. *Prog. Nucl. Magn. Reson. Spectrosc.* 11:211–272.
24. Marburger, S. P., B. M. Fung, and A. K. Khitrin. 2002. 14N chemical shifts and quadrupole coupling constants of inorganic nitrates. *J. Magn. Reson.* 154:205–209.
25. Smith, R., and E. Oldfield. 1984. Dynamic structure of membranes by deuterium NMR. *Science* 225:280–288.
26. Diehl, P., C. L. Khetrapal, and U. Lienhard. 1969. Deceptive simplicity in NMR spectra of oriented molecules. *Org. Magn. Reson.* 1:93–99.
27. Luz, Z. 1985. *Dynamics of molecular processes by NMR in liquid crystalline solvents.* In Nuclear magnetic resonance of liquid crystals. J. W. Emsley, editor. Springer Netherlands, Dordrecht. 315–342.

Chapter 2: Ceramide-C16 is a versatile modulator of phosphatidylethanolamine polymorphism**

2.1 Abstract

Ceramide-C16 (CerC16) is a sphingolipid associated with several diseases like diabetes, obesity, Parkinson disease, and certain types of cancers. As a consequence, research efforts are devoted to identify the impact of CerC16 on the behavior of membranes, and to understand how it is involved in these diseases. In this work, we investigated the impacts of CerC16 (up to 20 mol%) on the lipid polymorphism of 1-palmitoyl-2-oleoyl-*sn*-glycero-3-phosphoethanolamine (POPE), using differential scanning calorimetry, and sequential ^{2}H and ^{31}P solid-state NMR spectroscopy. A partial phase diagram is proposed. The results indicate that the presence of CerC16 leads to an up-shift of the temperature of the gel-to-liquid crystalline (L_β–L_α) phase transition, leading to a large L_β/L_α phase coexistence region where gel-phase domains contain ~35 mol% CerC16. It also leads to a down-shift of the temperature of the lamellar-to-inverted hexagonal (L–H_{II}) phase transition of POPE. The opposite influence on the two phase transitions of POPE brings a three-phase coexistence line when the two transitions overlap. The resulting H_{II} phase can be ceramide-enriched, coexisting with a L_α phase, or ceramide-depleted, coexisting with a L_β phase, depending on the CerC16 proportions. The uncommon capability of CerC16 to modulate the membrane fluidity, its curvature propensity, and the membrane interface properties highlights its potential as a versatile messenger in cell membrane events.

** Mahmoudreza Doroudgar and Michel Lafleur. *Biophysical Journal*, http://dx.doi.org/10.1016/j.bpj.2017.04.047

2.2 Introduction

Ceramides are bioactive sphingolipids that play an important role in cellular signaling and mediate several biological processes (1-9). For example, they are shown to be involved in some cellular events, including apoptosis (10-12), and in biological pathways leading, for example, to insulin resistance, and obesity (13, 14). In mammalian cell membranes, the most abundant acyl chains born by ceramides are saturated and contain 16 to 24 carbons (1, 15). The ceramide functions are intimately associated with their acyl chain length (10, 16). Among this family, ceramide with a palmitoyl chain (N-palmitoyl-D-erythro-sphingosine: CerC16) has been specifically shown to have a central influence in some cellular events. Because of the biological key roles of these molecules, it is essential to gain a detailed understanding of the modulation of the properties of biological membranes by ceramides; in the present work, we focussed our effort on characterizing the impact of CerC16 on the membrane physical properties.

From a chemistry point of view, ceramides display a relatively small polar head group that has the capability of forming hydrogen bonds through both the hydroxyl groups, and the amide linkage. As a consequence, ceramides with saturated acyl chains exhibit a dense molecular packing and have relatively high gel (L_β)-to-fluid (L_α) phase transition temperatures (T_m) in comparison to phospholipids (17). For instance, CerC16 undergoes a chain-melting transition at ~91 ^oC (18, 19). The impacts of ceramides on phospholipid bilayer properties have been recently reviewed (20, 21). These impacts are highly dependent on the ceramide chain length (19, 22-24). In general, when mixed with phospholipids, long-chain ceramides lead to an increase of the L_β–L_α phase transition temperature; this shift was observed for different binary lipid mixtures

including 1,2-dierucoyl-*sn*-glycero-3-phosphoethanolamine (DEPE) (19, 25), 1-palmitoyl-2-oleoyl-*sn*-glycero-3-phosphocholine (POPC) (24, 26-28), 1,2-dimyristoyl-*sn*-glycero-3-phosphocholine (DMPC) (29), and 1,2-dipalmitoyl-*sn*-glycero-3-phosphocholine (DPPC) (30). Moreover, ceramides induce a considerable broadening of the L_β–L_α phase transition, a phenomenon observed for binary mixtures of phosphatidylcholines (PC) and of phosphatidylethanolamine (PE) (19, 24, 26). This effect leads to a large phase-coexistence region in the phase diagrams where ceramide-rich gel-phase domains are found with ceramide-depleted fluid domains (19, 24, 26). The strong inter-ceramide interactions have been identified as the driving force leading to the formation of these gel-phase ceramide-enriched domains (26). Ceramides also lead to an increase in chain order of fluid bilayers as reported by studies using solid-state deuterium nuclear magnetic resonance (^{2}H-NMR) (22, 26, 31), and diphenylhexatriene fluorescence depolarization techniques (27, 28, 32). It was proposed that phase separations could also be observed at low temperatures, leading to the formation of two co-existing gel phases containing different ceramide proportions (19, 23, 26).

In addition to their effect on lateral mixing of lipids, ceramides have been shown to have an impact on the polymorphic propensities and curvature properties of bilayers; this phenomenon can be an alternative manner to modulate membrane properties. CerC16 (19), egg-yolk, and brain ceramides (25), bearing mainly C16 and C18 saturated chains, respectively, cause a decrease in the L_α-to-inverted hexagonal (H_{II}) phase transition temperature (T_H) of DEPE. For example, the addition of 10 mol% CerC16 brings T_H down from 66 ^{o}C for pure DEPE to 56 ^{o}C (19). Differential scanning calorimetry (DSC) results showed that the endotherm peak associated with this transition becomes broader in the presence of CerC16. The promotion of the H_{II} phase by

ceramide has been associated with its small head group, and with its extensive capability of forming H bonds (19). Because of their opposite effects on the two transitions (increasing T_m while decreasing T_H), ceramides can lead to an overlap of the L_β–L_α, and the L_α–H_{II} transitions (19). The presence of ceramides in bilayers formed by either PE, PC, or a mixture of both, was shown to induce membrane fusion and leakage; these phenomena were associated with the fact that ceramides could facilitate the formation of non-lamellar phases (33-36). It has also been proposed that ceramides promote the formation of non-lamellar intermediates because they display a rapid transbilayer motion (flip-flop) (37). Moreover, enzymatically produced ceramides cause the budding of giant unilamellar vesicles, and this formation of smaller vesicles was linked to the propensity of ceramides to acquire non-lamellar phases (38). Despite the fact that the ability of CerC16 to promote the H_{II} phase is established, there is a limited knowledge relative to the molecular details of inserted CerC16 in this lipid matrix.

In the present work, we employed DSC, and sequentially acquired ^2H and ^{31}P solid-state NMR techniques to study the impacts of CerC16 on the polymorphism of 1-palmitoyl-2-oleoyl-*sn*-glycero-3-phosphoethanolamine (POPE). The CerC16 proportion was varied between 0 and 20 mol%; this range covers membrane concentrations observed in physiologically relevant conditions – for example, ceramide content in mitochondria increases considerably during apoptosis and can reach 10% of total lipids (39, 40). Moreover it has been reported that metastable phases that are sensitive to hydration, and thermal history can be formed above 20 mol% (26). By using CerC16 bearing a fully deuterated palmitoyl chain (N-palmitoyl-d_{31}-D-erythro-sphingosine: CerC16-d_{31}), ^2H NMR spectra provided a quantitative characterization of the phases in which CerC16 was involved as well as a description of the ceramide chain order. In

parallel, ^{31}P chemical shielding anisotropy (CSA) of POPE provided a description of the phase behavior of the phospholipid. We carried out a sequentially acquisition of the ^{2}H, and ^{31}P NMR spectra of POPE/CerC16-d_{31} mixtures in defined and controlled conditions, including temperature. These data allowed a detailed description of the mixture phase behavior. A mirror sample with POPE bearing a fully deuterated palmitoyl chain (POPE-d_{31}) was also examined, not only to validate the phase behavior of POPE in the mixtures, but also to compare the order of POPE acyl chain with that of CerC16.

2.3 Materials and Methods

2.3.1 Materials

POPE, POPE-d_{31}, CerC16, and CerC16-d_{31} were purchased from Avanti Polar Lipids, Inc. (Alabaster, AL, USA). All the lipids were > 99% pure, and were utilized without further purification. 4-(2-Hydroxyethyl)piperazine-1-ethanesulfonic acid (HEPES, > 99%), ethylenediaminetetraacetic acid (EDTA, > 99%), and deuterium-depleted water (≤ 1 ppm deuterium oxide) were purchased from Sigma-Aldrich (St. Louis. MO, USA). NaCl (high purity grade) was supplied by AMRESCO LLC (Solon, OH, USA). Benzene (> 99%) and methanol (HPLC grade) were acquired from EMD Millipore Corporation (Billerica, MA, USA) and Fisher Scientific (Fair Lawn, NJ, USA), respectively.

2.3.2 Lipid Mixture Dispersions

The lipid mixtures were prepared from organic solutions. For the DSC measurements, a solution of CerC16 with a known concentration was first prepared by dissolving a weighted

quantity of CerC16 into an exact volume of a 90/10 (v/v) benzene/methanol mixture. Binary lipid mixtures with the desired composition were prepared by dissolving a weighted quantity of POPE into the appropriate volume of the CerC16 solution. The resulting solutions were freeze-dried for at least 24 hours to ensure the complete solvent elimination. For the NMR samples, the binary lipid mixtures were prepared by dissolving the appropriate quantities of POPE, and CerC16 into the 90/10 (v/v) benzene/methanol mixture and by freeze-drying the solution for at least 24 hours.

The lipid mixtures were hydrated using a HEPES buffer (20 mM HEPES, 100 mM NaCl, and 0.05 mM EDTA, prepared in Milli-Q water), pH 7.4. For the DSC experiments, the final lipid concentration was ~20 mM, except for the pure POPE dispersion for which the concentration was 7.8 mM. For the NMR samples, ~8 mg (~14 μmol) of CerC16-d_{31} were used for ensuring a good ^{2}H-NMR signal. A ~200-μL aliquot of buffer was used to hydrate each sample. Thus, the final lipid concentration varied from 703 mM for the POPE/CerC16-d_{31} 95/5 mixture, to 350 mM for the molar ratio 80/20. In the case of the POPE-d_{31}/CerC16 90/10 dispersion, 12 mg (16 μmol) POPE-d_{31}, 38 mg (53 μmol) POPE, and 4 mg (8 μmol) CerC16 were used, and the final lipid concentration was 384 mM. The same hydration protocol was performed for both DSC and NMR techniques: two heating-cooling cycles between 45 ^{o}C, and 0 ^{o}C, and a third cycle between 95 ^{o}C, and 0 ^{o}C were imposed on each lipid sample.

2.3.3 DSC Measurements

The DSC measurements were carried out on a VP-DSC MicroCalorimeter (MicroCal, Inc., Northampton, MA, USA). Three consecutive heating scans between 5, and 85 ^{o}C in the case of the pure POPE dispersion, and between 5, and 95 ^{o}C for the binary lipid mixtures, were carried

out at a heating rate of 30 ^{o}C/hour. The second and third scans provided very similar thermograms, and the second heating scans were selected for the analysis.

2.3.4 NMR Spectroscopy

The spectra were recorded using a Bruker Avance II 400 WB spectrometer equipped with a 9.4 T magnet, leading to a resonance frequency of 61.43 MHz and 162.03 MHz for ^{2}H and ^{31}P nucleus, respectively. A Bruker static probe with a 5-mm coil was used. In the case of ^{2}H acquisitions, five thousand scans were recorded using the quadrupolar echo pulse sequence with a 90^{o} pulse of 1.7 μs, an interpulse delay of 40 μs, and a recycle time of 300 ms. For the ^{31}P nucleus, a single 90^{o} pulse of 4.05 μs, a recycle delay of 1 s, and a "Waltz65" low-power proton decoupling were used for recording the spectra; typically, 1500 scans were recorded. The sequential acquisition of ^{2}H and ^{31}P NMR spectra was carried out as a function of temperature, between 0 ^{o}C, and ~65 °C. After the temperature stabilization, the signal acquisition of either nucleus was initiated. After the acquisition of the first spectrum, the spectrometer was then tuned for the signal acquisition of the other nucleus. The probe that was used presented the advantage of being tuned for the different nuclei without having to be removed from the magnet; this aspect was essential in the sequential acquisition of the NMR spectra as it kept the samples in the very same conditions during the data collection. At the phase transition temperatures, the spectrum of the first recorded nucleus was duplicated after the signal acquisition of the second nucleus, to validate that no significant phase evolution could be observed.

Based on the ^{2}H spectra, the phase distribution of CerC16 could be determined, as described in the Results and Discussion section. In a similar way, the ^{31}P NMR spectra provided a

description of the phase distribution of POPE as discussed below. The smoothed order profiles of the lipid acyl chains were obtained from the dePaked (41) ^{2}H-NMR spectra using the method previously described (42).

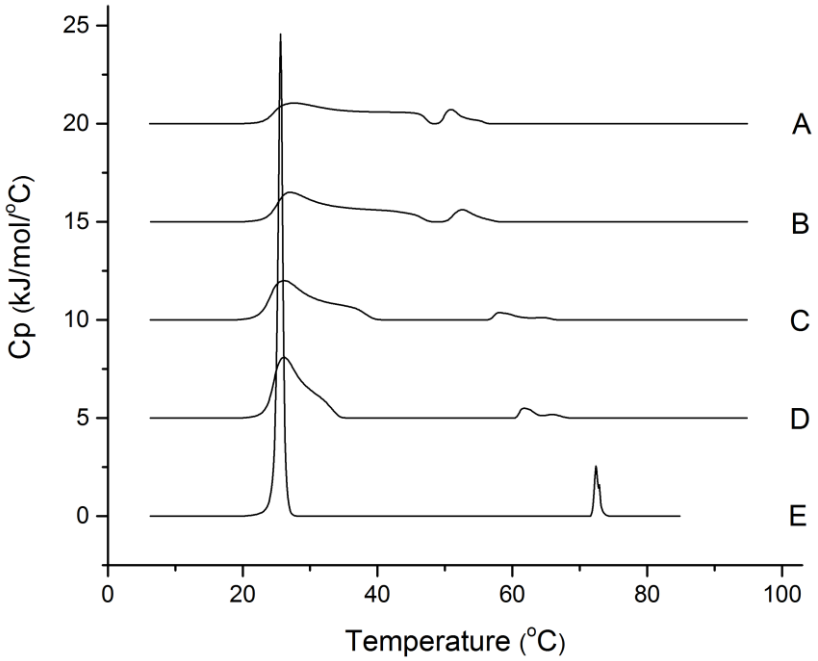

Fig. 2.1: DSC thermograms of POPE/CerC16 dispersions: (A) 80/20, (B) 85/15, (C) 90/10, (D) 95/05, and (E) pure POPE dispersion. To enhance the clarity, the thermograms were offset by 5 kJ/mol/^{o}C.

2.4 Results and Discussion

2.4.1 DSC Measurements

The DSC thermograms of a pure POPE dispersion and of POPE/CerC16 dispersions of various compositions are shown in Fig. 2.1. POPE displayed a L_β–L_α phase transition at 25 ^{o}C (T_m) whereas the L_α–H_{II} phase transition was observed at 72 ^{o}C (T_H). CerC16 disturbed significantly the

phase behavior of POPE, even at a molar fraction of 5 mol%. The presence of CerC16 resulted in two major impacts on the thermogram of a POPE dispersion: first, a broadening, and an up-shift in temperature of the endothermic $L_\beta - L_\alpha$ transition peak, and second, a broadening and a down-shift in temperature of the lamellar (L)$-H_{II}$ transition peak. The molar enthalpies of both phase transitions of pure POPE and of the investigated POPE/CerC16 dispersions are reported in Table 2.1. On one hand, CerC16 induced a decrease in the ΔH of the $L_\beta - L_\alpha$ transition, reducing it from 23.9 kJ/mol for pure POPE, which is in good agreement with the literature (43), to ~17.5 kJ/mol when the proportion of ceramide was between 5, and 20 mol%. On the other hand, CerC16 appeared to have no considerable influence on the ΔH of the $L-H_{II}$ transition as the values obtained for the investigated ceramide contents remained around 2.2 kJ/mol, a value observed for pure POPE dispersions (44). These results were analogous to those reported for DEPE/CerC16 mixtures (19), as well as for DEPE/egg-ceramides mixtures (25).

Table 2.1: The $L_\beta - L_\alpha$, and $L-H_{II}$ phase transition temperatures and enthalpies of a pure POPE dispersion and POPE/CerC16 dispersions of various molar fractions. The ΔH values are reported per mole of lipids i.e. POPE+CerC16. T_m, and T_H correspond to the top of the endothermic peaks.

POPE/CerC16 (mol ratio)	**T_m** (^oC)	ΔH **($L_\beta - L_\alpha$)** (kJ/mol)	**T_H** (^oC)	ΔH **($L-H_{II}$)** (kJ/mol)
100/00	25.6	23.9	72.4	2.2
95/05	26.0	17.9	61.7	1.6
90/10	26.2	17.5	58.1	1.8
85/15	26.9	18.3	52.6	2.4
80/20	27.4	16.9	50.8	2.4

2.4.2 NMR Spectroscopy

The sequential ^{2}H and ^{31}P NMR spectra of POPE/CerC16-d_{31} dispersions of various compositions are shown in Figs. 2.2, and Anx 1 (Annex). As mentioned above, ^{2}H and ^{31}P NMR spectra provided independent information about the phase characteristics of CerC16-d_{31} and POPE, respectively. For ^{31}P NMR, the CSA is representative of the different phospholipid phases. For instance, at 10 ^{o}C, the ^{31}P spectra of the lipid dispersions showed a CSA of ~69 ppm, a value characteristic of a gel lamellar phase. At 42 ^{o}C, the CSA was reduced to ~44 ppm and the spectra were typical of fluid systems (45, 46). The spectra indicated the shift of the L_{β}–L_{α} phase transition towards high temperatures as the ^{31}P-NMR spectra recorded in the L_{β}/L_{α} coexistence region displayed CSA values intermediate between those observed in the pure L_{β}, and the pure L_{α} phases; for example, at 42 ^{o}C, the spectrum of 20 mol% CerC16 mixture (CSA of 47 ppm) was broader than that of 10 mol% CerC16 dispersion (CSA of 45 ppm). ^{31}P-NMR spectra of phospholipids in the H_{II} phase display a CSA reduction by a factor of ~2, and an inversion of their line shape because of the rapid diffusion of the lipid molecules around the cylinders (46, 47). The shift of the L_{α}–H_{II} phase transition towards low temperatures in the presence of CerC16 was also observed by ^{31}P-NMR spectroscopy. For example, the spectrum recorded at 58 ^{o}C for the mixture containing 10 mol% CerC16 displayed a coexistence of the L_{α}, and H_{II} patterns whereas that at 57 ^{o}C for the mixture containing 15 mol% CerC16 was practically exclusively representative of the H_{II}. For the samples containing 15, and 20 mol% CerC16, a small narrow peak at 0 ppm was observed at high temperatures; it could correspond to the formation of a cubic phase, or small lipid assemblies. This narrow component always corresponded to less than 10% of the ^{31}P spectra

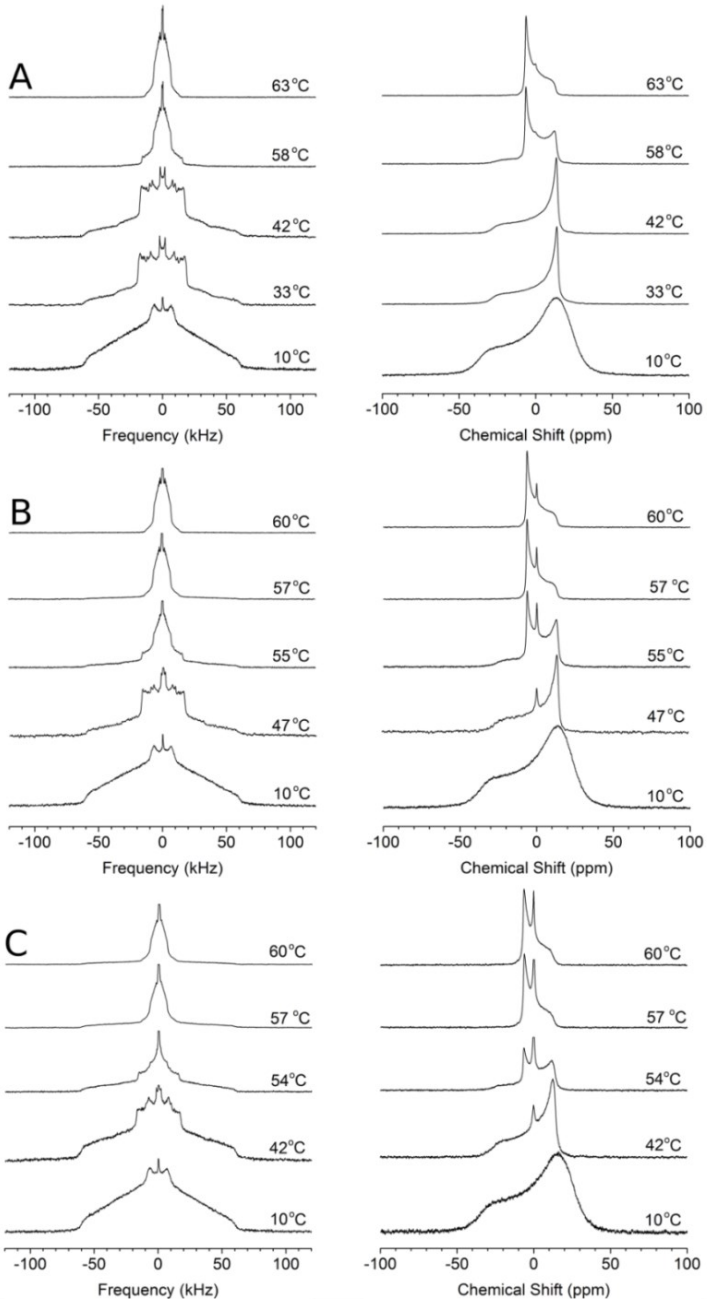

Fig. 2.2: The ^{2}H (left column) and ^{31}P (right column) NMR spectra of POPE/CerC16-d_{31} dispersions with various molar ratio: (A) 90/10, (B) 85/15, and (C) 80/20. The acquisition temperature is indicated on the right. The narrow peaks at 0 kHz in the ^{2}H-NMR spectra at high temperature were topped to allow a good representation of the H_{II} signal.

area. The formation of these structures was reversible as no such narrow component was observed in the spectra recorded at 25 ^{o}C after the heating run. In the case of ^{2}H-NMR, a broad featureless spectrum characteristic of a gel phase (48), was obtained at 10 ^{o}C for all the lipid dispersions. Upon heating, there was the apparition of a pattern representative of the L_{α} phase. This pattern was composed of several overlapping powder patterns with different quadrupolar splittings associated with the orientational order gradient existing along the lipid perdeuterated acyl chain (42, 48, 49). The ^{2}H-NMR spectra indicated a shift towards higher temperatures of the L_{β}–L_{α} phase transition experienced by CerC16-d_{31}. Several spectra were a superposition of L_{β}-, and L_{α}-phase components and it was observed from those recorded at 42-47 ^{o}C that the proportion of the L_{β}-phase component increased with increasing CerC16 content. Upon further heating, a profile associated with the H_{II} phase was observed. This pattern displayed quadrupolar splittings reduced by a factor of more than 2 compared to that of L_{α} phase (50). The overall shape was also different to that of the L_{α}-phase component because the symmetry of the H_{II} phase led to a more linear decrease of orientational order along the lipid chain. The spectra of all the dispersions at ~65-68 ^{o}C corresponded to the H_{II} pattern. These spectra included, as for the ^{31}P-NMR spectra, a small narrow peak centered at 0 kHz, representative of ceramides experiencing isotropic motions on the NMR time scale. This component represented at the maximum 5% of the area. Three observations must be highlighted. First, the spectra recorded at 54-55 ^{o}C for the POPE/CerC16-d_{31} mixtures with 15, and 20 mol% CerC16 were a superposition of components typical of the L_{β}, L_{α}, and H_{II} phases, revealing the coexistence of these 3 phases. Second, the spectra at 58 ^{o}C of the POPE/CerC16-d_{31} mixtures with a molar ratio of 95/5 and 90/10 included L_{α}-, and H_{II}-phase components whereas those of the 85/15, and 80/20 POPE/CerC16-d_{31} mixtures

at 57 °C was composed of the L_β-, and H_{II}-phase components. Third, all the CerC16 molecules were solubilized in the H_{II} phase upon heating as inferred from the ^{2}H-NMR spectra showing a single profile characteristic of the H_{II} phase.

We proceeded to a quantitative analysis of the spectra to determine the composition of the various phases. Since the lamellar, and H_{II} phases lead to distinct ^{2}H- and ^{31}P-NMR signals, the proportion of CerC16 (bearing the deuterated chain), and POPE (bearing the phosphate-containing head group) in each phase was inferred from the areas of the two components that could reproduce the experimental spectra by a linear combination. The components of the pure phases corresponded to experimental spectra acquired under different conditions (generally at a slightly different temperature and/or with a different CerC16 content). The area of the narrow peaks was determined directly on the spectra. In the case of ^{2}H-NMR spectra, the L_β, and L_α phases also led to 2 different profiles that could be resolved. Therefore, the distribution of CerC16-d_{31} between the different lamellar phases was inferred from the relative area of each component whose linear combination led to the best fit of the experimental spectra. The spectra typical of the pure phases were again obtained experimentally under different conditions leading to the presence of a single phase. The phase composition graphs of the binary lipid dispersions obtained from this quantitative analysis are presented in Fig. Anx 2.

Sequential ^{2}H- and ^{31}P-NMR was also used to determine the phase behavior of a POPE-d_{31}/C16-Cer 90/10 dispersion (Fig. 2.3). The phase composition analysis from the ^{2}H- and ^{31}P-NMR spectra was carried out using the approach described above; in this case, both nuclei probed the phase behavior of POPE in the mixture. For the L_α and H_{II} phases, the ^{2}H- and ^{31}P-NMR results provided a similar phase description, with an average difference of 5%. These were

also consistent with those provided by the ^{31}P-NMR of the POPE/CerC16-d_{31} mirror sample. The inferred phase distribution at 57-58 ^{o}C displayed a difference of 20% between the mirror samples, illustrating the observation that the L_{α}-H_{II} phase transition was very sensitive to the experimental conditions. This susceptibility also confirms that sequential NMR acquisition, as carried out in the present work, is essential to describe accurately the behavior of the labelled species. The fractions of POPE in the L_{β}, and L_{α} phases were obtained from the ^{2}H NMR spectra of POPE-d_{31}, as described above (Fig. Anx 3).

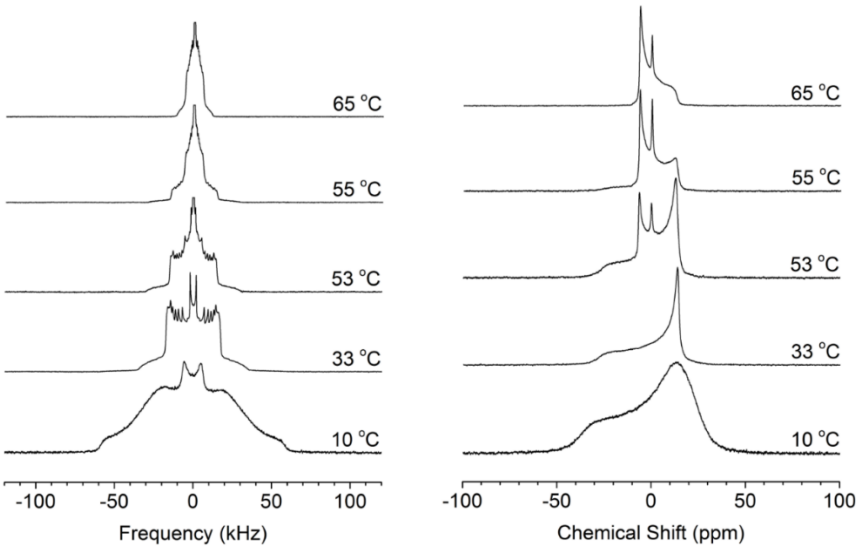

Fig. 2.3: The ^{2}H (left) and ^{31}P (right) NMR spectra of a POPE-d_{31}/CerC16 90/10 dispersion.

The combination of the NMR and DSC data led to the construction of the partial phase diagram of POPE/CerC16 system (Fig. 2.4). This diagram does not take into account the contribution of the narrow line in the NMR spectra as this was always a small component and its assignment could not be clearly established. The onset of the L_{β}-L_{α} phase transition of the investigated POPE/CerC16 mixtures was very similar for the different proportions of CerC16,

suggesting the existence of a three-phase line and, consequently, a gel/gel phase coexistence region. The existence of ceramide-rich, and ceramide-depleted domains is also reflected by the solidus line that is considerably different to the one predicted from regular solution theory (51), (see Fig. Anx 4). It is noteworthy that the gel-phase NMR spectra of POPE-d_{31}/CerC16 mixtures at 10 ^{o}C displayed slightly more pronounced components at $\pm$20 kHz than that of POPE/CerC16-d_{31} mixtures (Figs. 2.2, and 2.3), suggesting a slightly faster rotational diffusion (52). This observation would be compatible with POPE involved in a more dynamic gel phase than CerC16. The two spectra showed however a single and similar component for the CD_3 signal; therefore, the methyl dynamics appeared to be not sufficiently different to be resolved in the spectra. A gel/gel phase coexistence region was also observed for DEPE/CerC16 (19), POPC/CerC16 (26), and PSM/CerC16 (53) phase diagrams. AFM experiments revealed the existence of two gel phases with distinct nanomechanical properties in PSM/CerC16 (53), and DPPC/CerC16 mixtures (54). Moreover 1,1'-dioctadecyl-3,3,3',3'-tetramethylindocarbocyanine perchlorate (DiIC18), a lipophilic fluorescent probe, was found to partition differently between two gel phases.

The DSC results indicated an upshift of the L_β–L_α transition temperature as a function of the CerC16 proportion in the lipid mixture, and the NMR results showed that both lipids experienced this upshift. The coexistence phase regions reflect well the asymmetrical shape of the endotherms in the DSC thermograms. The solidus (the frontier between the L_β, and the L_β/L_α regions), and the liquidus (the frontier between the L_β/L_α, and the L_α regions) lines could be determined from the ^{2}H-NMR spectra, using the method introduced by Vist et al. (55) and successfully applied to N-palmitoyl-sphingomyelin (PSM)/CerC16 mixtures (53). This subtraction method was applied using the ^{2}H-NMR spectra obtained from the mixtures containing 10, and 20

mol% CerC16-d_{31}. The results indicated that between 30 ^{o}C and 50 ^{o}C, L_{α}-phase domains containing ~5 mol% CerC16 coexisted with L_{β}-phase domains that contained ~30 mol% CerC16. The L_{β}/L_{α} phase distributions of POPE, and of CerC16 obtained from the two series of mirror-sample ^{2}H-NMR spectra (Figs. 2.1, 2.2, Anx 1, Anx 2 and Anx 3) were put together to infer the composition of each phase, providing an alternative method to determine the solidus and the liquidus boundaries from a different data set. The agreement between the liquidus lines obtained from the spectral subtraction method (55) and from the phase distributions in the mirror samples was very good. The later method determined that the gel-phase domains included ~40 mol% CerC16, a value slightly higher than that inferred from the spectral subtraction method. This difference is likely within the experimental error associated with the uncertainties in the subtraction factors, the area determinations, and the sample compositions.

At 54–55 ^{o}C, the coexistence of three phases ($L_{\beta}/L_{\alpha}/H_{II}$) could be assessed from the ^{2}H-NMR spectra. The L_{β} phase appeared to involve exclusively CerC16 while the L_{α}, and H_{II} phases were a mixture of the two lipids. Since the investigated lipid mixtures included two components (water was in excess in all the dispersions), a 3-phase horizontal line must be included in the phase diagram. This line was extended up to only 20 mol% CerC16, as we do not have sufficient information to describe the behavior for larger CerC16 contents. Moreover, the phase behavior of phospholipid bilayers containing higher CerC16 proportions is somehow controversial because of the presence of putative metastable phases (18, 26). The NMR results revealed that the nature of transition towards the H_{II} phase was deeply affected by the CerC16 content. The lipid mixtures underwent a transition from L_{α} phase to H_{II} phase when their CerC16 content was less than ~10 mol% whereas a L_{β} phase coexisting with the H_{II} phase was observed when the CerC16 content

was 15, and 20 mol%. This finding led to the inclusion of an eutectic point where L_{β}, L_{α}, and H_{II} phases should coexist.

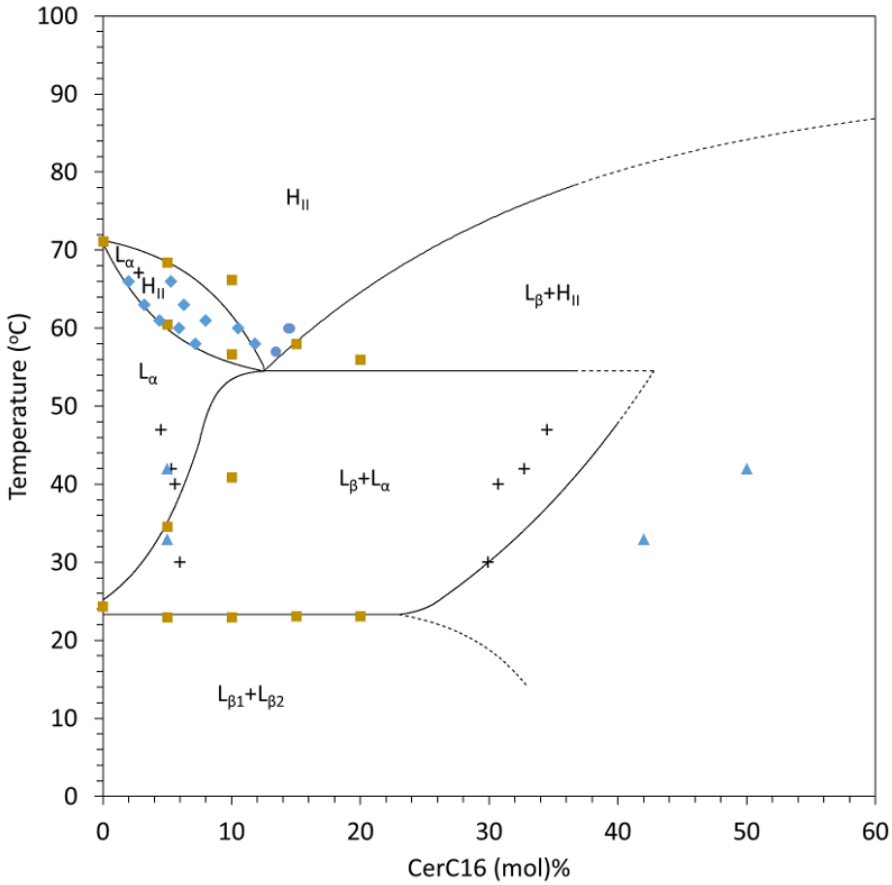

Fig. 2.4: The proposed partial phase diagram for POPE/CerC16 system. The brown squares define both the onsets and ends of the endothermic transitions obtained by DSC. The plus signs indicate the solidus and the liquidus lines inferred from the spectral subtraction method introduced by Vist et al. (55) The blue triangles indicate the solidus and liquidus lines derived from the lipid distributions obtained from the ^{2}H-NMR spectral simulation of the POPE/CerC16 90/10 mirror samples. The blue diamond symbols define the frontiers of the L_{α}/H_{II} coexistence region inferred from the lipid distributions obtained from the sequential ^{2}H-, and ^{31}P-NMR spectra of the POPE/CerC16-d_{31} 90/10 mixture. The blue circles define the frontiers of the L_{β}/H_{II} coexistence region inferred from the lipid distributions obtained from the sequential ^{2}H-, and ^{31}P-NMR spectra of POPE/CerC16-d_{31} 85/15, and 80/20 mixtures.

The compositions determined from the ^{2}H- and ^{31}P-NMR spectra (Figs. Anx 2 and Anx 3) defined the boundaries of the L_{α}/H_{II}, and L_{β}/H_{II} phase co-existence regions. There is a general good agreement between the DSC and NMR results. Small differences in transition temperatures were observed, a phenomenon that could be associated with the use of deuterated CerC16 in the case of the NMR samples (53, 55), with the fact that NMR data were (assumed to be) acquired at equilibrium, with stepwise temperature increments whereas DSC data were collected during continuous heating, and that the sample thermal history could not be identical. The main discrepancy between the results obtained by the 2 techniques was related to the $L–H_{II}$ phase transition of the mixture with 20 mol% CerC16, where ^{2}H-NMR results indicate a co-existence of the L_{β} and H_{II} phases over a wider temperature range. As previously pointed out, the NMR, and DSC techniques do not reproduce the very same conditions and the $L_{\alpha}–H_{II}$ phase transition is particularly sensitive to such variations.

This is, to the best of our knowledge, the first proposal of a partial phase diagram for POPE/CerC16 system. Some features should be compared with those previously proposed for systems including CerC16, and a phospholipid. The POPE/CerC16 phase diagram includes a relatively large L_{β}/L_{α} phase coexistence region. The fluid domains include about 5 mol% CerC16 while the L_{β}-phase domains contain about 35 mol%. The compositions of the gel-phase domains are consistent with those observed for the PSM/CerC16 system (53, 56). This similar behavior adds to the understanding of the driving force leading to the phase separation. It has been proposed that the capacity of ceramide head group to make H bonds, both as an acceptor and a donor, leads to strong inter-ceramide interactions and promotes phase separation (53, 56, 57). POPE head group has also an extensive H-bond capability as a donor and an acceptor because of

its quaternary ammonium. Despite the H-bond capacity of POPE, a phase separation was still observed in the POPE/CerC16 system. It is proposed that the absence of a phosphate group, reducing considerably the effective size of the head group (POPE molecular area: 0.74 nm^2 (58), CerC16 molecular area: 0.40 nm^2 (30, 59)), plays a major role in the phase separation, leading to a closer proximity of the molecules and therefore, stronger intermolecular interactions.

A distinctive part of the POPE/CerC16 phase diagram is the 3-phase line that leads to L_β/H_{II}, and L_α/H_{II} phase coexistence regions. This feature is a consequence of the opposite effect of CerC16 on the transitions: it leads to the existence of the L_β phase at higher temperatures, and, at the same time, to the formation of H_{II} phase at lower temperatures. The overlap of the L_β-L_α, and L_α-H_{II} phase transitions was previously observed for DEPE/CerC16 system at a molar proportion $10 < x \leq 20$ (mol%) (19). It should be pointed out that for 10 mol% CerC16 and below, the H_{II} phase, when coexisting with the L_α phase, was enriched in CerC16. It is inferred that its relatively small head group favored the formation of an inverted non lamellar phase. Conversely, for the mixtures with > 15 mol% CerC16, the H_{II} cylinders were depleted in CerC16 relative to the overall content. This behavior reflected the ordering effect of this lipid and its propensities to form gel phase. The present work clearly establishes the L_β-H_{II} phase transition for mixtures containing ≥ 15 mol% CerC16. Such a transition was mentioned for DEPE/CerC16 system (19), and for partly dehydrated egg-PE (60). Recently it was shown that egg ceramide (40 to 60 mol%) in egg sphingomyelin would also lead to a L_β-H_{II} phase transition observed at high temperature (~70 ^oC) (61). In POPE/CerC16 system, this transition could be associated with the fact that the increase in temperature leads to the disordering of CerC16 acyl chains, promoting the cone shape

of the lipid, and to an enhanced solubilisation of CerC16 in the existing H_{II} phase mainly formed by POPE.

The ^{2}H-NMR spectroscopy of the mirror samples also provided the characterization of the dynamics of the lipid acyl chains in the POPE/CerC16 90/10 mixture. The smoothed order profiles of ceramide (derived from the mixture containing CerC16-d_{31}) as well as of POPE (derived from the mixture containing POPE-d_{31}) acyl chains are presented in Fig. 2.5 for the L_α and H_{II} phases.

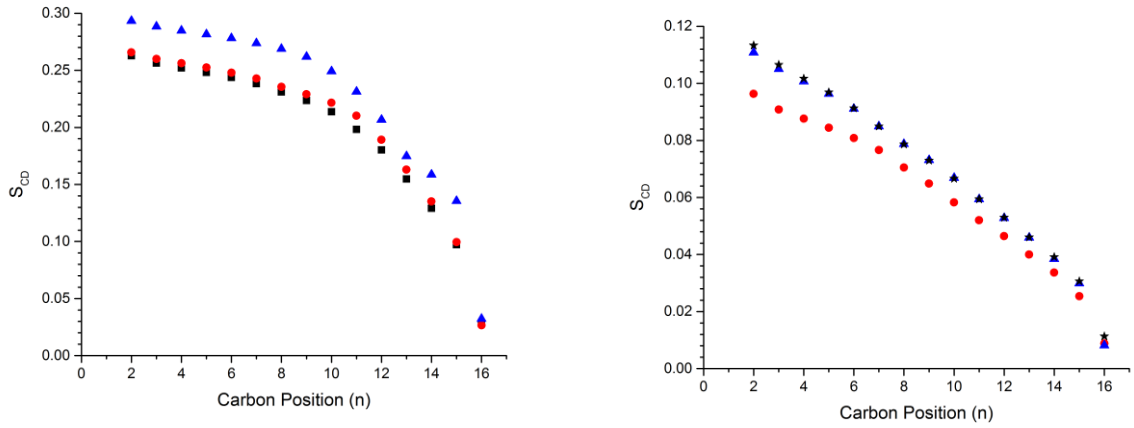

Fig. 2.5: Smoothed order profiles of POPE-d_{31} and CerC16-d_{31} in the L_α (left, at 42 ^{o}C) and the H_{II} (right, at 65 ^{o}C) phase. **Left:** POPE/CerC16-d_{31} 90/10 (blue triangles), POPE-d_{31}/CerC16 90/10 (red circles), and pure POPE-d_{31} (black squares). **Right:** POPE/CerC16-d_{31} 80/20 (black stars), POPE/CerC16-d_{31} 80/10 (blue triangles), and POPE-d_{31}/CerC16 90/10 (red circles).

The L_α order profiles of both CerC16 and POPE, typical of the liquid-lamellar phase, consisted of a plateau associated with the carbons near to the lipid head group, followed by a sharp decrease of order towards the end of the chain. The profiles revealed that in the POPE/CerC16 90/10 mixture, the chain order parameters of CerC16 were noticeably higher than those of POPE. This observation is similar with the results obtained for POPC/CerC16 mixtures

(26), where the palmitoyl chain of POPC was found less ordered than that of CerC16. An orientational order of the ceramide palmitoyl chain greater than that of PC was also deduced from a molecular dynamics simulation of the DMPC/CerC16 system (62). Therefore, even though the binary mixtures were likely homogeneous in the L_α phase, the palmitoyl chain of CerC16 and that of the phospholipid did not have the same orientational order. It has been proposed that the limited molecular area associated with CerC16 would leave a limited space for chain conformational disordering (26). Alternatively, it may be associated with the position of the head group relative to the bilayer normal. It has been recently shown (64) that the orientational order parameters of fatty acid chains in bilayers are modulated by the protonation state of the carboxylic group; deprotonated acid groups are more exposed to the aqueous environment and this location leads to higher chain order parameters. The small head group of CerC16 combined with its capability of making H bonds may position this lipid head group at a higher level than PE head groups. This organization would lead, similar to the unprotonated fatty acid (64), to a larger overall orientational order.

The presence of ceramide appears to have a limited impact on the orientational order of POPE acyl chain (Fig. 2.5), in contrast with its significant ordering effect on POPC acyl chain (26). It should be highlighted that pure POPE L_α-phase bilayers exhibit already a relatively high chain order because of the limited head group size as well as its capacity to make H bonds between ethanolamine group (49). The ordering effect of CerC16 on fluid phospholipid bilayers is likely limited when the bilayer existing order is considerable. In fact, it has been shown that cholesterol has a less pronounced ordering effect on POPE than on POPC fluid bilayers (63); it appears that CerC16 behaves similarly.

The acyl chain order profiles in the H_{II} phase have also been determined (Fig. 2.5B). As expected (50), the order decrease along the chain was more linear than in the case of the L_α phase; this was observed for the chains of both POPE, and CerC16. These ^{2}H-NMR profiles are a solid evidence that the ceramide molecules were inserted in the H_{II} cylinders. The ratios $S(L_\alpha)/S(H_{II})$ were 2.7 close to the head group and were 4.0 near the end of the palmitoyl chain; these values were similar for the palmitoyl chain of POPE and of CerC16. These ratios were also consistent with those reported for pure POPE (50). This reduction is associated with the diffusion of the lipid molecules around the H_{II} cylinders, a motion that causes additional averaging of the quadrupolar interactions, as well as with the different lipid phase symmetry. Similar to the L_α phase, CerC16 displayed higher chain order parameters compared to those of POPE in the H_{II} phase formed by the POPE/CerC16 90/10 mixture. It is unlikely that the difference in chain order between POPE, and CerC16 could be due to a phase separation within the H_{II} cylinders. A position of CerC16 head group closer to the H_{II} cylinder center than that of POPE head group could be the origin of the orientational order difference.

2.5 Conclusions

In the present work, the proposed partial phase diagram of the POPE/CerC16 system shows that CerC16 has a compound impact: it can act as a versatile modulator, being able to promote L_β or H_{II} phase, and to lead to ceramide-enriched (coexisting with L_α phase) or ceramide-depleted (coexisting with L_β phase) H_{II} cylinders. In some specific conditions (in the case of POPE/CerC16 mixture, at about 10 mol% CerC16 and 54 ^{o}C), these propensities are regulated by small changes in temperature and/or CerC16 proportion. It should be pointed out that these effects are

reported to be buffered by cholesterol. For example, the formation of ceramide-rich gel-like domains was hampered in the presence of cholesterol (20, 65, 66). Similarly, the gel-phase domains existing in phospholipid bilayers at low CerC16 contents (e.g. 5 mol% in the current work) were not observed when 10 mol% CerC16 were added to red blood cell (RBC) lipid extract. However, phase separations were observed when the CerC16 content was increased to 30 mol% or when the RBC lipid extract was cholesterol depleted (67). This being said, local fluctuations of the lipid compositions in biological membranes could lead to gel-phase domains as those reported in the present work. Both CerC16, and cholesterol (up to 30 mol%) (63), promote the formation of the H_{II} phase. At this point, their combined effect is not established but local variations of these species are bound to modulate the local curvature of membranes. It is well established that the order of a bilayer core and the polymorphic propensities of membranes have a pivotal role in controlling protein activity and consequently, many cellular processes (68, 69). As an example, it has been shown that Bax proteins are involved in the perturbation of the permeability of outer mitochondrial membranes, a phenomenon associated with apoptosis. The pore formation associated with these proteins is modulated by the curvature properties and the fluidity of the membrane (70-72). The variation of CerC16 content in membranes can be a way to control the membrane association, and the aggregation of Bax proteins and therefore could play a pivotal role in the modulation of the membrane permeability and apoptosis. The fact that CerC16 can modulate bilayer order, curvature propensities, domain formation, and the chemistry of the interface suggest that it could act as a versatile messenger in cellular processes.

2.6 References:

1. Pewzner-Jung, Y., S. Ben-Dor, and A. H. Futerman. 2006. When do lasses (longevity assurance genes) become cers (ceramide synthases)?: Insights into the regulation of ceramide synthesis. *J. Biol. Chem.* 281:25001–25005.
2. Gómez-Muñoz, A. 1998. Modulation of cell signalling by ceramides. *Biochim. Biophys. Acta.* 1391:92–109.
3. Uchida, Y. 2014. Ceramide signaling in mammalian epidermis. *Biochim. Biophys. Acta.* 1841:453–462.
4. Hannun, Y. A., C. R. Loomis, . . ., R. M. Bell. 1986. Sphingosine inhibition of protein kinase C activity and of phorbol dibutyrate binding in vitro and in human platelets. *J. Biol. Chem.* 261:12604–12609.
5. Hsieh, C. T., J. H. Chuang, . . ., Y. Lin. 2014. Ceramide inhibits insulin-stimulated Akt phosphorylation through activation of Rheb/mTORC1/S6K signaling in skeletal muscle. *Cell. Signal.* 26:1400–1408.
6. Karunakaran, U., J. S. Moon, . . ., K. C. Won. 2015. CD36 initiated signaling mediates ceramide-induced TXNIP expression in pancreatic beta-cells. *Biochim. Biophys. Acta.* 1852:2414–2422.
7. Merrill, A. H., A. M. Sereni, . . ., J. M. Kinkade. 1986. Inhibition of phorbol ester-dependent differentiation of human promyelocytic leukemic (HL-60) cells by sphinganine and other long-chain bases. *J. Biol. Chem.* 261:12610–12615.
8. Rahman, A., F. Thayyullathil, . . ., S. Galadari. 2016. Hydrogen peroxide/ceramide/Akt signaling axis play a critical role in the antileukemic potential of sanguinarine. *Free Radical Biol. Med.* 96:273–289.
9. Teixeira, V., T. C. Medeiros, . . ., V. Costa. 2016. Ceramide signaling targets the PP2A-like protein phosphatase Sit4p to impair vacuolar function, vesicular trafficking and autophagy in Isc1p deficient cells. *Biochim. Biophys. Acta.* 1861:21–33.
10. Grösch, S., S. Schiffmann, and G. Geisslinger. 2012. Chain length-specific properties of ceramides. *Prog. Lipid Res.* 51:50–62.
11. Mesicek, J., H. Lee, . . ., R. Kolesnick. 2010. Ceramide synthases 2, 5, and 6 confer distinct roles in radiation-induced apoptosis in HeLa cells. *Cell. Signal.* 22:1300–1307.
12. Sassa, T., S. Suto, . . ., A. Kihara. 2012. A shift in sphingolipid composition from C24 to C16 increases susceptibility to apoptosis in HeLa cells. *Biochim. Biophys. Acta.* 1821:1031–1037.
13. Turpin, S. M., H. T. Nicholls, . . ., J. C. Brüning. 2014. Obesity-induced CerS6-dependent C16:0 ceramide production promotes weight gain and glucose intolerance. *Cell Metab.* 20:678–686.
14. Raichur, S., . . ., S. A. Summers. 2014. CerS2 haploinsufficiency inhibits β-oxidation and confers susceptibility to diet-induced steatohepatitis and insulin resistance. *Cell Metab.* 20:687–695.
15. Bouhours, J. F., and H. Guignard. 1979. Free ceramide, sphingomyelin, and glucosylceramide of isolated rat intestinal cells. *J. Lipid Res.* 20:897–907.
16. Park, W.-J., and J.-W. Park. 2015. The effect of altered sphingolipid acyl chain length on various disease models. *Biol. Chem.* 396:693–705.

17. Maula, T., M. Kurita, . . ., J. P. Slotte. 2011. Effects of sphingosine 2N- and 3O-methylation on palmitoyl ceramide properties in bilayer membranes. *Biophys. J.* 101:2948–2956.

18. Shah, J., J. M. Atienza, . . ., G. G. Shipley. 1995. Structural and thermotropic properties of synthetic C16:0 (palmitoyl) ceramide: Effect of hydration. *J. Lipid Res.* 36:1936–1944.

19. Sot, J., F. J. Aranda, . . ., A. Alonso. 2005. Different effects of long- and short-chain ceramides on the gel-fluid and lamellar-hexagonal transitions of phospholipids: A calorimetric, NMR, and X-ray diffraction study. *Biophys. J.* 88:3368–3380.

20. Castro, B. M., M. Prieto, and L. C. Silva. 2014. Ceramide: A simple sphingolipid with unique biophysical properties. *Prog. Lipid Res.* 54:53–67.

21. Goñi, F. M., J. Sot, and A. Alonso. 2014. Biophysical properties of sphingosine, ceramides and other simple sphingolipids. *Biochem. Soc. Trans.* 42:1401–1408.

22. Huang, H. W., M. E. Goldberg, and R. Zidovetzki. 1998. Ceramides perturb the structure of phosphatidylcholine bilayers and modulate the activity of phospholipase A2. *Eur. Biophys. J.* 27:361–366.

23. Pinto, S. N., L. C. Silva, . . ., M. Prieto. 2011. Effect of ceramide structure on membrane biophysical properties: The role of acyl chain length and unsaturation. *Biochim. Biophys. Acta.* 1808:2753–2760.

24. Pinto, S. N., L. C. Silva, . . ., M. Prieto. 2008. Membrane domain formation, interdigitation, and morphological alterations induced by the very long chain asymmetric C24:1 ceramide. *Biophys. J.* 95:2867–2879.

25. Veiga, M. P., J. L. R. Arrondo, . . ., A. Alonso. 1999. Ceramides in phospholipid membranes: Effects on bilayer stability and transition to nonlamellar phases. *Biophys. J.* 76:342–350.

26. Hsueh, Y. W., R. Giles, . . ., J. Thewalt. 2002. The effect of ceramide on phosphatidylcholine membranes: A deuterium NMR study. *Biophys. J.* 82:3089–3095.

27. Silva, L., R. F. M. De Almeida, . . ., M. Prieto. 2006. Ceramide-platform formation and -induced biophysical changes in a fluid phospholipid membrane. *Mol. Membr. Biol.* 23:137–148.

28. Holopainen, J. M., M. Subramanian, and P. K. J. Kinnunen. 1998. Sphingomyelinase induces lipid microdomain formation in a fluid phosphatidylcholine/sphingomyelin membrane. *Biochemistry.* 37:17562–17570.

29. Holopainen, J. M., J. Lemmich, . . ., P. K. J. Kinnunen. 2000. Dimyristoylphosphatidylcholine/C16:0-ceramide binary liposomes studied by differential scanning calorimetry and wide- and small-angle X-ray scattering. *Biophys. J.* 78:2459–2469.

30. Carrer, D. C., and B. Maggio. 1999. Phase behavior and molecular interactions in mixtures of ceramide with dipalmitoylphosphatidylcholine. *J. Lipid Res.* 40:1978–1989.

31. Huang, H. W., E. M. Goldberg, and R. Zidovetzki. 1996. Ceramide induces structural defects into phosphatidylcholine bilayers and activates phospholipase A2. *Biochem. Biophys. Res. Commun.* 220:834–838.

32. Holopainen, J. M., J. Y. A. Lehtonen, and P. K. J. Kinnunen. 1997. Lipid microdomains in dimyristoylphosphatidylcholine–ceramide liposomes. *Chem. Phys. Lipids.* 88:1–13.

33. Ruiz-Argüello, M. B., G. Basáñez, . . ., A. Alonso. 1996. Different effects of enzyme-generated ceramides and diacylglycerols in phospholipid membrane fusion and leakage. *J. Biol. Chem.* 271:26616–26621.

34. Ruiz-Argüello, M. B., F. M. Goñi, and A. Alonso. 1998. Vesicle membrane fusion induced by the concerted activities of sphingomyelinase and phospholipase C. *J. Biol. Chem.* 273:22977–22982.

35. Sot, J., F. M. Goñi, and A. Alonso. 2005. Molecular associations and surface-active properties of short- and long-N-acyl chain ceramides. *Biochim. Biophys. Acta.* 1711:12–19.

36. Ruiz-Argüello, M. B., M. P. Veiga, . . ., A. Alonso. 2002. Sphingomyelinase cleavage of sphingomyelin in pure and mixed lipid membranes. Influence of the physical state of the sphingolipid. *Chem. Phys. Lipids.* 114:11–20.

37. Contreras, F. X., G. Basañez, . . ., F. M. Goñi. 2005. Asymmetric addition of ceramides but not dihydroceramides promotes transbilayer (flip-flop) lipid motion in membranes. *Biophys. J.* 88:348–359.

38. Holopainen, J. M., M. I. Angelova, and P. K. J. Kinnunen. 2000. Vectorial budding of vesicles by asymmetrical enzymatic formation of ceramide in giant liposomes. *Biophys. J.* 78:830–838.

39. Hannun, Y. A. 1996. Functions of ceramide in coordinating cellular responses to stress. *Science.* 274:1855–1859.

40. Dai, Q., J. Liu, . . ., R. M. Lee. 2004. Mitochondrial ceramide increases in UV-irradiated HeLa cells and is mainly derived from hydrolysis of sphingomyelin. *Oncogene.* 23:3650–3658.

41. Bloom, M., J. H. Davis, and A. L. Mackay. 1981. Direct determination of the oriented sample NMR spectrum from the powder spectrum for systems with local axial symmetry. *Chem. Phys. Lett.* 80:198–202.

42. Lafleur, M., B. Fine, . . ., M. Bloom. 1989. Smoothed orientational order profile of lipid bilayers by 2H-nuclear magnetic resonance. *Biophys. J.* 56:1037–1041.

43. Pozo Navas, B., K. Lohner, . . ., G. Pabst. 2005. Composition dependence of vesicle morphology and mixing properties in a bacterial model membrane system. *Biochim. Biophys. Acta.* 1716:40–48.

44. Epand, R. M. 1985. High sensitivity differential scanning calorimetry of the bilayer to hexagonal phase transitions of diacylphosphatidylethanolamines. *Chem. Phys. Lipids.* 36:387–393.

45. Niederberger, W., and J. Seelig. 1976. Phosphorus-31 chemical shift anisotropy in unsonicated phospholipid bilayers. *J. Am. Chem. Soc.* 98:3704–3706.

46. Seelig, J. 1978. 31P nuclear magnetic resonance and the head group structure of phospholipids in membranes. *Biochim. Biophys. Acta.* 515:105–140.

47. Cullis, P. R., and B. De Kruijff. 1979. Lipid polymorphism and the functional roles of lipids in biological membranes. *Biochim. Biophys. Acta.* 559:399–420.

48. Davis, J. H. 1983. The description of membrane lipid conformation, order and dynamics by 2H-NMR. *Biochim. Biophys. Acta.* 737:117–171.

49. Lafleur, M., P. R. Cullis, and M. Bloom. 1990. Modulation of the orientational order profile of the lipid acyl chain in the Lα phase. *Eur. Biophys. J.* 19:55–62.

50. Lafleur, M., P. R. Cullis, . . ., M. Bloom. 1990. Comparison of the orientational order of lipid chains in the Lalpha and HII phases. *Biochemistry.* 29:8325–8333.

51. Heimburg, T. 2007. *Thermal biophysics of membranes.* Wiley-VCH Verlag GmbH & Co. KGaA.

52. Jansson, M., R. L. Thurmond, . . ., M. F. Brown. 1992. Deuterium NMR study of intermolecular interactions in lamellar phases containing palmitoyllysophosphatidylcholine. *J. Phys. Chem.* 96:9532–9544.

53. Leung, S. S., J. V. Busto, . . ., J. Thewalt. 2012. Insights into sphingolipid miscibility: Separate observation of sphingomyelin and ceramide N-acyl chain melting. *Biophys. J.* 103:2465–2474.

54. García-Arribas, A. B., J. V. Busto, . . ., F. M. Goñi. 2015. Atomic force microscopy characterization of palmitoylceramide and cholesterol effects on phospholipid bilayers: A topographic and nanomechanical study. *Langmuir.* 31:3135–3145.

55. Vist, M. R., and J. H. Davis. 1990. Phase equilibria of cholesterol/dipalmitoylphosphatidylcholine mixtures: Deuterium nuclear magnetic resonance and differential scanning calorimetry. *Biochemistry.* 29:451–464.

56. Busto, J. V., M. L. Fanani, . . ., A. Alonso. 2009. Coexistence of immiscible mixtures of palmitoylsphingomyelin and palmitoylceramide in monolayers and bilayers. *Biophys. J.* 97:2717–2726.

57. Slotte, J. P. 2016. The importance of hydrogen bonding in sphingomyelin's membrane interactions with co-lipids. *Biochim. Biophys. Acta.* 1858:304–310.

58. Garcia-Manyes, S., Ò. Domènech, . . ., J. Hernandez-Borrell. 2007. Atomic force microscopy and force spectroscopy study of langmuir–blodgett films formed by heteroacid phospholipids of biological interest. *Biochim. Biophys. Acta.* 1768:1190–1198.

59. Löfgren, H., and I. Pascher. 1977. Molecular arrangements of sphingolipids. The monolayer behaviour of ceramides. *Chem. Phys. Lipids.* 20:273–284.

60. Castresana, J., J. L. Nieva, . . ., A. Alonso. 1992. Partial dehydration of phosphatidylethanolamine phosphate groups during hexagonal phase formation, as seen by IR spectroscopy. *Biochem. J.* 282:467–470.

61. Barriga, H. M. G., E. S. Parsons, . . ., N. J. Brooks. 2015. Pressure–temperature phase behavior of mixtures of natural sphingomyelin and ceramide extracts. *Langmuir.* 31:3678–3686.

62. Dutagaci, B., J. Becker-Baldus, . . ., C. Glaubitz. 2014. Ceramide–lipid interactions studied by MD simulations and solid-state NMR. *Biochim. Biophys. Acta.* 1838:2511–2519.

63. Paré, C., and M. Lafleur. 1998. Polymorphism of POPE/cholesterol system: A 2H nuclear magnetic resonance and infrared spectroscopic investigation. *Biophys. J.* 74:899–909.

64. Paz Ramos, A., P. Lagüe, . . ., M. Lafleur. 2016. Effect of saturated very long-chain fatty acids on the organization of lipid membranes: A study combining 2H NMR spectroscopy and molecular dynamics simulations. *J. Phys. Chem. B.* 120:6951–6960.

65. Massey, J. B. 2001. Interaction of ceramides with phosphatidylcholine, sphingomyelin and sphingomyelin/cholesterol bilayers. *Biochim. Biophys. Acta.* 1510:167–184.

66. Busto, J. V., J. Sot, . . ., A. Alonso. 2010. Cholesterol displaces palmitoylceramide from its tight packing with palmitoylsphingomyelin in the absence of a liquid-disordered phase. *Biophys. J.* 99:1119–1128.

67. García-Arribas, A. B., H. Ahyayauch, . . ., F. M. Goñi. 2016. Ceramide-induced lamellar gel phases in fluid cell lipid extracts. *Langmuir.* 32:9053–9063.

68. Battle, A. R., P. Ridone, . . ., B. Martinac. 2015. Lipid–protein interactions: Lessons learned from stress. *Biochim. Biophys. Acta.* 1848:1744–1756.

69. Lee, A. G. 2004. How lipids affect the activities of integral membrane proteins. *Biochim. Biophys. Acta.* 1666:62–87.

70. Basañez, G., J. C. Sharpe, . . ., J. Zimmerberg. 2002. Bax-type apoptotic proteins porate pure lipid bilayers through a mechanism sensitive to intrinsic monolayer curvature. *J. Biol. Chem.* 277:49360–49365.

71. Gilbert, R. J. C. 2016. Protein–lipid interactions and non-lamellar lipidic structures in membrane pore formation and membrane fusion. *Biochim. Biophys. Acta.* 1858:487–499.

72. Mignard, V., L. Lalier, . . ., F. M. Vallette. 2014. Bioactive lipids and the control of bax pro-apoptotic activity. *Cell Death Dis.* 5:e1266.

Chapter 3: Characterization of n-decane distribution within phosphatidylethanolamine L_α/H_{II} phases

3.1 Introduction

The spontaneous curvature (SC) of a lipid membrane is expressed under zero bending stress condition (1). Lipids whose SC involves a non zero curvature need to modify their molecular morphologies to be able to build bilayers of zero curvature. This modification imposes stress on the bilayers. For instance, while cylindrical-shaped POPC molecules make relaxed bilayers of zero SC (or infinite intrinsic radius of curvature,R_0), cone-shaped POPE molecules need to compress their acyl chains to adapt cylindrical morphologies so they can form bilayers of zero curvature. This morphological modification stores on the bilayers "elastic free energy" that induces the bilayers to adapt non-bilayer H_{II} phase at some higher temperature (71 ^oC in the case of POPE) in which the lipid molecules can retrieve their cone-shaped conformation and release the stored elastic free energy (1).

The H_{II} phase involves tightly packed cylindrical monolayers and void spaces in between. Since the existence of void spaces is thermodynamically unfavorable as it causes the loss of entropy, some phospholipids molecules have to stretch their acyl chains to fill the void spaces (1). Therefore, the L_α–H_{II} transition of POPE bilayers is dictated by the balance between the expression of$R_0$and the creation of interstitial voids.

Alkanes of different chain lengths can promote the formation of H_{II} phase and decrease the$T_H$of various PE systems (1-5) . It has been suggested that alkanes have the capability of filling

the interstitial void spaces between the H_{II} cylinders, releasing the cylinder packing stress. Chen et al. (6) have investigated the impacts of the chain length of various alkanes on the H_{II} phase transition of DOPE. They concluded that, in the H_{II} phase, short chain alkanes, such as decane, are mostly located in the phospholipid acyl chain region; therefore, they promote the L_α–H_{II} transition by decreasing$R_0$of the monolayer. However, longer chain alkanes, such as tetradecane, promote the L_α–H_{II} transition mainly by filling the interstitial spaces between the H_{II} phase cylinders, and thus, releasing the intercylinder packing stress.

As the second part of my M.Sc. project, I investigated the effects of 10 mol% n-decane, a short chain alkane, on the L_α–H_{II} transition of POPE. Similar to the first part, sequential ^2H and ^{31}P-NMR spectroscopy was employed for quantitatively describing the molecular distribution of the both components. I used perdeuterated n-decane (n-decane-d_{22}) so its distribution could be characterized by the ^2H-NMR spectra. POPE was probed by ^{31}P-NMR. The partitioning constant of n-decane between POPE L_α and H_{II} phases was determined.

3.2 Materials and Methods

3.2.1 Materials

N-decane-d_{22} (> 98 atom % D) was supplied by C/D/N ISOTOPES, Inc. (Pointe-Claire, QC, Canada). The other materials used in this part of the project including POPE, HEPES, EDTA, deuterium depleted water, NaCl, benzene, and methanol were already identified in section 2.3.1.

3.2.2 Lipid Mixture Dispersions

A POPE/n-decane-d_{22} 90/10 (mol)% mixture was prepared by directly adding 3.2 µL n-decane-d_{22} to 105.9 mg POPE. The lipid dispersion was then prepared by adding ~400 µL of HEPES buffer (20 mM HEPES, 100 mM NaCl, and 0.05 mM EDTA, pH 7.4, prepared in deuterium depleted water) to the lipid mixture. The hydration method was already described in the section 2.3.2. After centrifugation, the excess buffer was removed and the lipid dispersion was transferred into a NMR sample holder.

3.2.3 NMR Spectroscopy

The sequential ^{2}H and ^{31}P-NMR spectroscopy of a POPE/n-decane-d_{22} 90/10 mol% sample were performed using the parameters described in section 2.3.4. The ^{2}H-NMR spectra were dePaked using GRAMS software and through applying the method introduced by Bloom et al. (7). This operation enhances the resolution of the L_{α}/H_{II} components of a ^{2}H spectrum through eliminating the orientational dependency of the quadrupolar couplings and leaving only a signal typical of an oriented sample with an orientation perpendicular to the B_0 direction. The baseline correction and band fittings were carried out using OriginPro 9.2 software.

3.3 Results and Discussions

The ^{2}H and ^{31}P-NMR spectra of a POPE/n-decane-d_{22} 90/10 mol% mixture at different temperatures are shown in Figure 3.1. It is observed that 10 mol% n-decane had noticeable

effects on the POPE phase transition. The ^{31}P spectra clearly illustrated that the L_α–H_{II} transition was already initiated at 25 ^oC. At this temperature, the CSA of the major component was 45 ppm, a value characteristic of a phospholipid in L_α phase (8). The spectrum acquired at 25 ^oC, also included the components of H_{II} phase whose $\delta_\perp$ component could be observed around -6 ppm. The H_{II} components became more intense upon increase of temperature. The ^{31}P spectrum at 56 ^oC was characteristic of a phospholipid in H_{II} phase as it represented a reverse line shape compared to that of the L_α phase, and a CSA of 21 ppm which was slightly less than the half of that of the L_α phase spectrum (9, 10) . Hence, at 56 ^oC, it was only the H_{II} components remained as the spectrum, indicating that the L_α–H_{II} phase transition was complete. A very narrow component appeared ~0 ppm of the ^{31}P spectra indicating to the presence of an isotropic phase in the mixture. Its intensity was however very limited (covered less than 1% of the total spectrum area) and was not considered in the following analysis.

The ^2H-NMR spectra were representative of the n-decane behavior within the POPE/n-decane 90/10 mol% mixture. It should be noted that pure n-decane is in liquid state over the investigated temperature range of this project (25–56 ^oC). Except the one acquired at 56 ^oC that included only two powder patterns, the ^2H spectra included three distinct powder patterns; a wide powder pattern, a mid-width powder pattern, and a very narrow powder pattern; these could be visualized in more details on the dePaked ^2H spectra (Figure 3.1, third column). At 25 ^oC, the wide powder pattern had a quadrupolar splitting of 11.8 kHz, the middle one, 3.0 kHz, and the narrow one was so narrow that it could not be dePaked without artifacts. The Both wide and middle components became narrower with increasing temperature. For instance, at 47 ^oC, their widths were 8.6 kHz and 2.6 kHz, respectively.

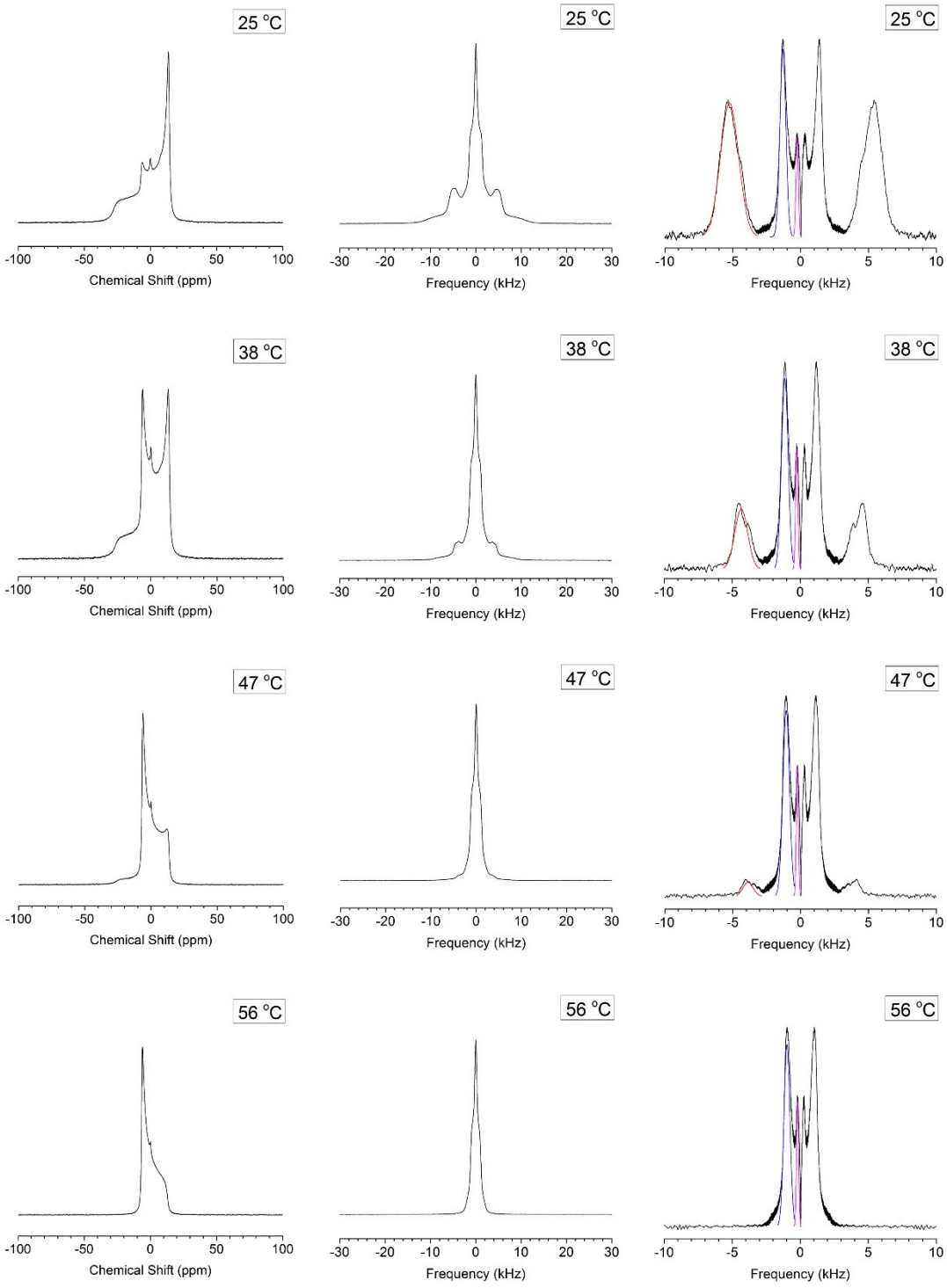

Fig. 3.1: The sequentially acquired (left column) ^{31}P- and (middle column) ^{2}H-NMR spectra of a POPE/n-decane-d_{22} 90/10 mol% dispersion. The dePaked spectra of the corresponding ^{2}H-NMR spectra are presented on right column. The fitted components of the dePaked spectra are plotted in different colors. See the text for more details.

Structurally, n-decane-d_{22} is a simple aliphatic chain consisted of ten carbon atoms including eight central methylene (C^2H_2) and two terminal methyl (C^2H_3). Since all the eight C^2H_2 are linked to two other carbon groups, their motions are more restricted than those of the two terminal C^2H_3 which are bounded only from one side. Therefore, the wider powder patterns were assigned to the eight C^2H_2 of n-decane-d_{22} in L_α phase, whereas the two terminal methyl (C^2H_3) contributed to the middle powder pattern. The mobility difference between the C^2H_2 and C^2H_3 groups was also observed in the ^{2}H-NMR spectra of CerC16-d_{31} and POPE-d_{31}, in Chapter 2. The narrower powder patterns, the ones included two overlapped narrow powder patterns and can be observed on all the ^{2}H spectrum, must be assigned to both the less restricted terminal C^2H_3 in L_α phase, and all the ten C^2H_2 and C^2H_3 groups in H_{II} phases. In other words, one could rationalize that while the corresponding area of the H_{II} phase components were increasing through increase of temperature, those of corresponding to the L_α phase decreased simultaneously. As also observed on the ^{31}P spectra, the very narrow powder patterns around 0 kHz should be correspond, though beside the very less restricted parts of n-decane in H_{II} phase, to the presence of n-decane in an isotropic phase. However, these two probable constituents of the narrowest powder patterns were not distinguishable as their relaxation time were longer than the signal recording time scale used in this experiment.

Globally, the ^{2}H spectra line shape of n-decane-d_{22} methylenes did not demonstrate the same superimposed powder patterns as those of CerC16-d_{31} in Chapter 2. As explained, the superimposed ^{2}H powder patterns of CerC16-d_{31} in L_α phase were due to the orientational order gradients along the CerC16-d_{31} perdeuterated acyl chains. It has been reported that when mixed with different PC, short chain alkanes such as hexane are located in the middle of the bilayers in

L_α phase, causing an increase in their thickness (11, 12) . The authors rationalized that the alkane molecules were probably located in the middle of the bilayers, penetrating into the lower part of the acyl chains. The quadrupolar splitting of the widest powder pattern of n-decane-d_{22} in POPE L_α phase at 47 ^oC corresponded to that of the last C^2H_2 and the terminal C^2H_3 along the acyl chain in pure POPE-d_{31} bilayers (13). This comparison suggests that n-decane-d_{22} molecules were located in a disordered environment in L_α phase, most likely localized in the middle of POPE bilayers in L_α phase. Because n-decane molecules appear to be localized in the lower part of POPE acyl chains, they increase the total volume of the acyl chain part of the bilayers while the polar head group volume remains the same, inducing the cone shape. Hence, this additional "packing stress" initiates the L_α–H_{II} transition at a much lower temperature (~25 ^oC).

The ^2H powder patterns width of n-decane-d_{22} in L_α phase were $\geq$ 3 folds wider than those of the H_{II} phase at the same temperature. As a comparison, this ratio was ~2 for CerC16-d_{31} (in chapter 2). A ratio of 2 is expected (14) and confirmed the inclusion of CerC16-d_{31} with POPE in H_{II} phase. However, the higher L_α/H_{II} powder pattern width ratios of n-decane-d_{22} infers that n-decane-d_{22} molecules could not only much be localized along to the POPE acyl chains in H_{II} phase, but included in an environment in which they experienced even lower degrees of restriction compared to those of the middle of the bilayers in L_α phase. Mixed with monomethylated dioleoylphosphatidylethanolamine (DOPE-Me) as the host phospholipid, Siegel et al. (15) have derived that , dodecane-d_{26} and hexadecane-d_{34}, as two rather long chain alkanes, were totally located within the interstitial spaces between the H_{II} phase cylinders. The authors' inference was based on the L_α/H_{II} powder pattern width ratios $\geq$ 5 for these two alkanes. Chen et al. (6) also concluded that long chain alkanes were mainly located between H_{II} cylinders. In my case, the

abovementioned ratio ≥ 3 obtained for n-decane-d_{22}, indicates that short chain alkanes, such as n-decane, could be localized somewhere between the interstitial spaces and the lower part of the phospholipid acyl chains in H_{II} phase. This inference is in good agreement with the conclusion obtained by Chen et al. (6).

As mentioned earlier, all the ^{2}H and ^{31}P-NMR spectra of the POPE/n-decane-d_{22} mixture, except those of acquired at 56 ^{o}C, consisted of overlapped L_{α}/H_{II} phase components. In case of the ^{31}P spectra, the subtraction method used for the analysis of the POPE/CerC16-d_{31} mixture spectra (chapter 2) was exploited for determining the distribution of POPE in either the two L_{α}/H_{II} phases. Briefly explained, I subtracted the pure H_{II} phase ^{31}P spectrum of POPE obtained at 56 ^{o}C from those of acquired at lower temperatures, then calculated the ratio of either the L_{α}/H_{II} phases through measuring their corresponding areas at each temperatures. However, for two reasons, I was not able to use the same subtraction method in case of the ^{2}H spectra. First, it was the powder pattern width variation of the H_{II} components through increase of temperature, which made it almost impossible to perform a precisely subtraction of the pure H_{II} spectrum acquired at 56 ^{o}C from each of those obtained at lower temperatures. The second reason was the lack of a pure L_{α} phase ^{2}H spectrum that is required for the subtraction. Consequently, I used the dePaked spectra (Figure 3.1, the third column).

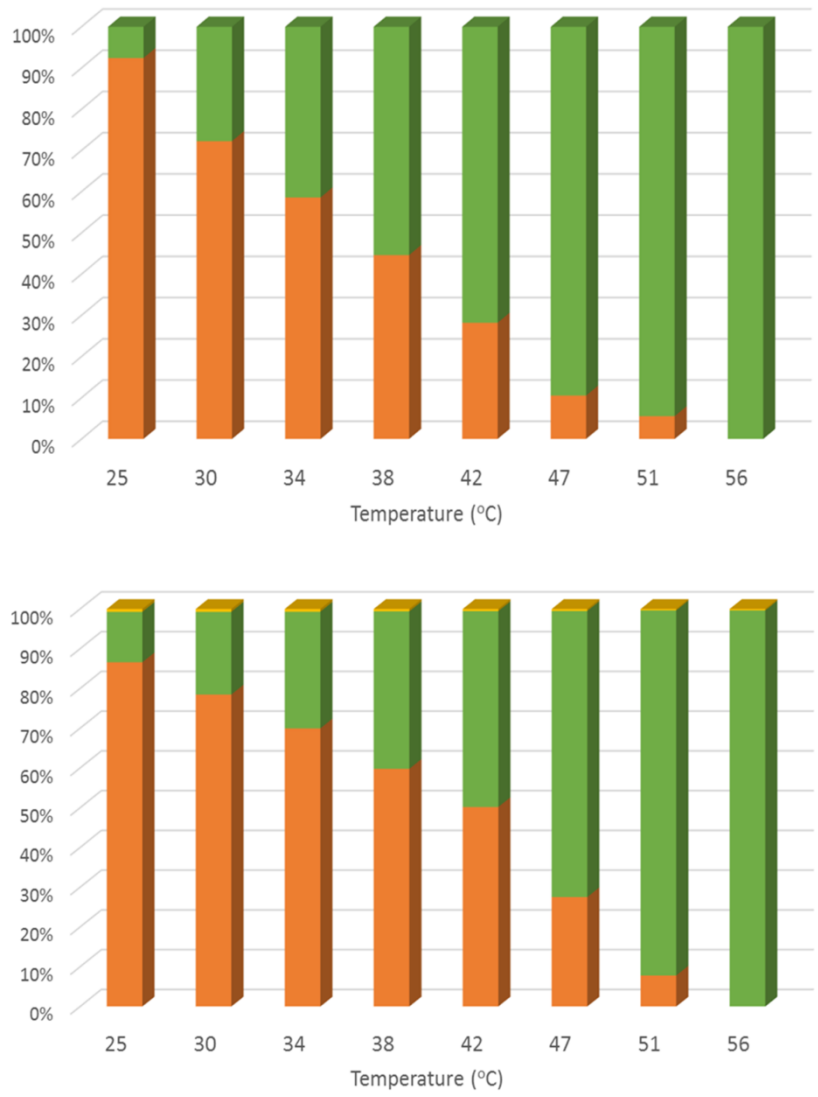

Fig. 3.2: Phase partitioning graphs of (top) n-decane-d_{22} and (bottom) POPE at different temperatures. Color guide: orange bars, green bars, and yellow bars represent L_α phase, H_{II} phase, and isotropic phase, respectively.

As described above, the dePaked ^2H spectra of n-decane-d_{22} at different temperatures displayed three different doublets. The one with the widest splitting must correspond to the eight C^2H_2 of n-decane-d_{22} in L_α phase. The intermediate one represents the superimposed components of

both the two terminal C^2H_3 in L_α phase and the eight C^2H_2 in H_{II} phase. The narrowest doublets are associated with a component with very high degree of freedom; it could be assigned to the two C^2H_3 of decane in H_{II} phase as well as some n-decane-d_{22} in an isotropic phase.

To determine the proportion of decane in the L_α/H_{II} phases, the doublets with the largest and the middle quadrupolar splittings were fitted using GaussAmp fit method. The area of the widest doublet corresponded to the eight C^2H_2 in the L_α phase. The intermediate doublet was assigned to the overlapped L_α–phase C^2H_3 and H_{II}–phase C^2H_2. The area associated with the two terminal C^2H_3 (i.e. 6 deuteriums) in L_α phase should equal 6/16 or 0.375 of the area of the largest doublet (which correspond to eight C^2H_2 or 16 deuteriums). By subtracting this component, I was able to estimate the area corresponding to the eight C^2H_2 in H_{II} phase.

Knowing the phase distribution of n-decane-d_{22} and POPE (Figure 3.2), it is possible to determine the partitioning constant of n-decane-d_{22} between the two L_α/H_{II} phases (*K*) at different temperatures, using Equation 3.1:

$$K = \frac{\left(X_{n-decane-d_{22}}/X_{POPE}\right)_{L_\alpha}}{\left(X_{n-decane-d_{22}}/X_{POPE}\right)_{H_{II}}} \qquad \textbf{Eq. } 3.1$$

where *X* is the relative proportion of either the lipid components in different phases. The *K* constants and the proportion of POPE in H_{II} phase were plotted versus temperature as shown in Figure 3.3. Except two temperature regions, the very beginning of the L_α–H_{II} and the one close to the end of the transition, in which the calculation uncertainties of *K* could have been high, the $K \leq 1$ at different temperatures indicates that H_{II} phase was favoured through increase of temperature.

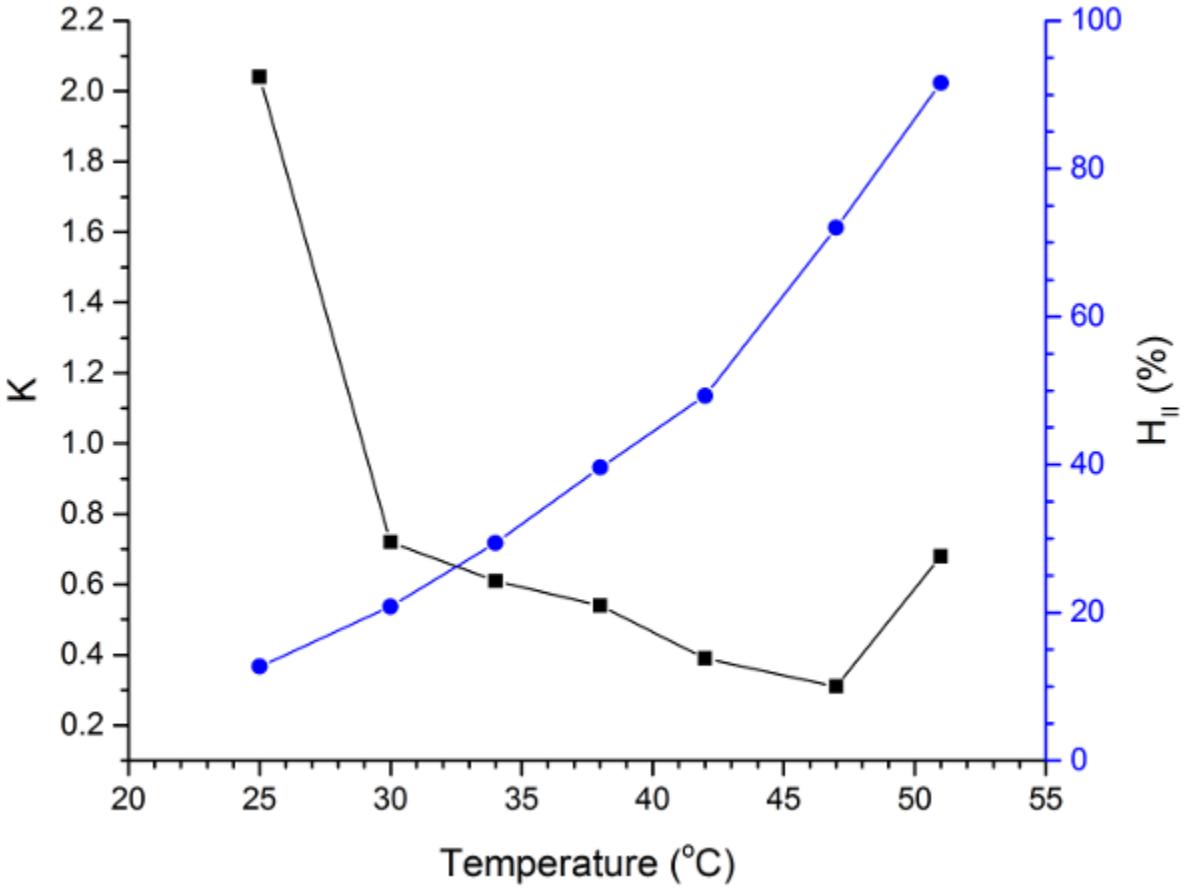

Fig. 3.3: The partitioning constant, K, (black squares) and POPE H_{II} phase content (blue circles) of the mixture at different temperatures. The data precision is ± 0.01 for K, and ± 2% for H_{II} proportion in temperature range of 30–47 °C.

Furthermore, the slightly decreasing of *K* as a function of temperature indicates to the sluggish progress of the L_α–H_{II} transition. Globally, there could be a balance between the two main factors pushing POPE bilayers to slightly accomplishing the L_α–H_{II} transition. In other words, while the packing stress over the POPE acyl chains was gradually decreasing since more and more n-decane molecules were transferred to H_{II} phase, at the same time, the kinetic motion of POPE molecules

was progressively raising, reaching to the specific level being necessary for accomplishment of the L_α–H_{II} transition. This could justify the slow progression of the L_α–H_{II} transition over a broad range of temperature.

It is noteworthy that when temperature raises, the lipid molecules receive some higher degree of freedom in H_{II} phase – faster diffusion around the H_{II} cylinders, which consequently shrinks the radius of the H_{II} cylinders, and as a result, the interstitial spaces. This may imply to an inconsistency with what the K constants demonstrates for the POPE/n-decane-d_{22} dispersion in this project, as the linear descending trend of *K* indicates to a continues transfer of n-decane-d_{22} to H_{II} phase. One inference could be explained based on the total volume of the interstitial spaces that can be created by a constant amount of lipid molecules in H_{II} phase. In fact, the same amount of lipid molecules could create some bigger H_{II} cylinders and interstitial spaces, or smaller, but more numerous cylinders and interstitial spaces. In other words, the total volume of the interstitial spaces could remain the same, no matter how the size of the H_{II} cylinders changes.

3.4 Conclusions

In this part of the project, the effects of 10 mol% n-decane on the polymorphism of POPE was investigated. N-decane promoted remarkably the L_α–H_{II} transition of POPE, shifting it toward lower temperatures. The end point of the transition was much less affected. It led to a transition broadness of ~30 ^oC. This downshifted transition is associated with the impacts of n-decane on the molecular packing of POPE in both L_α and H_{II} phases. Since n-decane molecules were located near the end of POPE acyl chains in the lamellar phase, they caused an increase on the packing

stress of the bilayers. The other impact of n-decane favoring the H_{II} phase is related to filling the unfavorable void spaces between the H_{II} cylinders. Globally, the two effects of the n-decane molecules – the high level of packing stress in L_α phase and the filled void spaces in H_{II} phase, made the POPE bilayers initiate the L_α–H_{II} transition at a much lower temperature. The sequential ^2H and ^{31}P solid-state NMR spectroscopy was a great approach for measuring the phase distribution of both n-decane-d_{22} and POPE in either the L_α/H_{II} phases under the very same conditions. This technique allowed to calculate the partitioning constant of the POPE/-n-decane-d_{22} mixture at different temperatures.

3.5 References

1. Gruner, S. M. 1985. Intrinsic curvature hypothesis for biomembrane lipid composition: A role for nonbilayer lipids. *Proc. Natl. Acad. Sci.* 82:3665–3669.
2. Gruner, S. M. 1989. Stability of lyotropic phases with curved interfaces. *J. Phys. Chem.* 93:7562–7570.
3. Tate, M. W., and S. M. Gruner. 1987. Lipid polymorphism of mixtures of dioleoylphosphatidylethanolamine and saturated and monounsaturated phosphatidylcholines of various chain lengths. *Biochemistry* 26:231–236.
4. Hornby, A. P., and P. R. Cullis. 1981. Influence of local and neutral anaesthetics on the polymorphic phase preferences of egg yolk phosphatidylethanolamine. *Biochim. Biophys. Acta* 647:285–292.
5. Rand, R. P., N. L. Fuller, . . ., and V. A. Parsegian. 1990. Membrane curvature, lipid segregation, and structural transitions for phospholipids under dual-solvent stress. *Biochemistry* 29:76–87.
6. Chen, Z., and R. P. Rand. 1998. Comparative study of the effects of several n-alkanes on phospholipid hexagonal phases. *Biophys. J.* 74:944–952.
7. Bloom, M., J. H. Davis, and A. L. Mackay. 1981. Direct determination of the oriented sample NMR spectrum from the powder spectrum for systems with local axial symmetry. *Chem. Phys. Lett.* 80:198–202.
8. Niederberger, W., and J. Seelig. 1976. Phosphorus-31 chemical shift anisotropy in unsonicated phospholipid bilayers. *J. Am. Chem. Soc.* 98:3704–3706.
9. Seelig, J., and J. L. Browning. 1978. General features of phospholipid conformation in membranes. *FEBS Lett.* 92:41–44.
10. Cullis, P. R., and B. De Kruijff. 1979. Lipid polymorphism and the functional roles of lipids in biological membranes. *Biochim. Biophys. Acta* 559:399–420.

11. Jacobs, R. E., and S. H. White. 1984. Behavior of hexane dissolved in dimyristoylphosphatidylcholine bilayers: An NMR and calorimetric study. *J. Am. Chem. Soc.* 106:915–920.
12. White, S. H., G. I. King, and J. E. Cain. 1981. Location of hexane in lipid bilayers determined by neutron diffraction. *Nature* 290:161–163.
13. Lafleur, M., P. R. Cullis, and M. Bloom. 1990. Modulation of the orientational order profile of the lipid acyl chain in the Lα phase. *Eur. Biophys. J.* 19:55–62.
14. Lafleur, M., P. R. Cullis, . . ., and M. Bloom. 1990. Comparison of the orientational order of lipid chains in the L.alpha. And HII phases. *Biochemistry* 29:8325–8333.
15. Siegel, D., J. Banschbach, and P. Yeagle. 1989. Stabilization of HII phases by low levels of diglycerides and alkanes: An NMR, calorimetric, and X-ray diffraction study. *Biochemistry* 28:5010–5019.

4 Conclusions

My M.Sc. project mainly focused on two subjects. In the first part, I investigated how CerC16 alters the polymorphism of POPE. Globally, CerC16 had two major impacts on the thermal behavior of POPE. It broadened the L_β–L_α phase transition and shifted it towards higher temperatures. It also broadened the L_α–H_{II} phase transition and shifted it towards lower temperatures. For a CerC16 content $\geq$ 12.5 mol%, the two phase transitions overlapped causing a coexistence of the three phases at ~54-55 ^oC. The order profile of both POPE and CerC16 acyl chains showed that, 10 mol% CerC16 did not have significant impacts on the order parameters of POPE acyl chain in L_α phase. However, the order parameters of CerC16 in both L_α/H_{II} phases are higher than those of POPE, a phenomenon that may be associated with a different level of CerC16 in the self-assembly or a smaller molecular area of this lipid.

As the second part of the project, I studied the impacts of n-decane on the polymorphism of POPE. The results showed that n-decane broadened significantly the L_α–H_{II} phase transition of POPE and shifted it towards lower temperatures; 10 mol% n-decane caused the transition to begin at ~25 ^oC and to end at ~56 ^oC. N-decane alters the polymorphism of POPE, first, through an increase in the stored elastic stress in POPE bilayers, and second, by filling the unfavorable interstitial void spaces between the cylinders in H_{II} phase, releasing the packing stress.

I employed the sequential ^2H and ^{31}P solid-state NMR spectroscopy as the main technique in the both parts of the project where I recorded one after another ^2H and ^{31}P signals, under the very same conditions. Although there have been several studies in which the authors exploited the solid-state NMR spectroscopy of either ^2H, or ^{31}P, or both but separately, it was the first time,

to the best of my knowledge, that the two techniques were utilized in a sequential way for studying the polymorphism of a lipid mixture. This approach was very advantageous as it provided some crucial information not only about the phase behavior of the both components, but also about the dynamic of the perdeuterated constituents under the very same lipid-composition and thermal conditions. A key component to setup this approach was the use of a probe that could be tuned for both nuclei without taking it out of the magnet. Removing the probe from the magnet leads to temperature variations and make it essentially impossible to obtain the very same conditions. The sequential acquisition of ^{2}H and ^{31}P spectra led to a partial phase diagram for the POPE/CerC16 system.

Sequential ^{2}H and ^{31}P-NMR spectroscopy of lipid mixtures is a simple approach to gain important information about the different phase behavior of the components of the mixture at a specific temperature. This technique could be easily exploited to study the impacts of other components of biological importance on phospholipid polymorphism. As two examples, one could characterize the impact of peptides and local anesthetics, two membrane active agents, on the lipid phase behavior. Peptides consist of approximately ≤ 50 amino acids. An important group of peptides – the cell penetrating peptides with hydrophobic structures, govern some of the most important activities of cell membranes, such as selective transportation of various species from/into the cells (1, 2). Some anesthetics attach to the sodium channel proteins within the neuron cell membranes, block the transmission of the nerve impulses and thus, cause the loss of local sensation. ^{2}H or ^{31}P-NMR spectroscopy have been separately utilized in several studies for investigating the role of these species in altering the phase behavior of cell membranes (3-9). By

taking advantage of sequential ^{2}H and ^{31}P-NMR spectroscopy, one can precisely track the effects of these molecules on the phase behavior of the phospholipid.

4.1 References

1. Milletti, F. 2012. Cell-penetrating peptides: Classes, origin, and current landscape. *Drug Discov. Today* 17:850–860.
2. Stalmans, S., E. Wynendaele, . . ., and B. De Spiegeleer. 2013. Chemical-functional diversity in cell-penetrating peptides. *PLoS One* 8:e71752.
3. Morein, S., R. E. Koeppe Ii, . . ., and J. Antoinette Killian. 2000. The effect of peptide/lipid hydrophobic mismatch on the phase behavior of model membranes mimicking the lipid composition in escherichia coli membranes. *Biophys. J.* 78:2475–2485.
4. Sherman, P. J., F. Separovic, and J. H. Bowie. 2014. The investigation of membrane binding by amphibian peptide agonists of CCK2R using 31P and 2H solid-state NMR. *Peptides* 55:98-102.
5. Naito, A., T. Nagao, . . ., and H. Saitô. 2002. Dynorphin induced magnetic ordering in lipid bilayers as studied by 31P NMR spectroscopy. *Biochim. Biophys. Acta* 1558:34–44.
6. Fillion, M., M. Noël, . . ., and M. Auger. 2014. Investigation of the mechanism of action of novel amphipathic peptides: Insights from solid-state NMR studies of oriented lipid bilayers. *Biochim. Biophys. Acta* 1838:2173–2179.
7. Song, C., H. Lygre, and W. Nerdal. 2008. Articaine interaction with DSPC bilayer: A 13C and 31P solid-state NMR study. *Eur. J. Pharm. Sci.* 33:399–408.
8. Weizenmann, N., D. Huster, and H. A. Scheidt. 2012. Interaction of local anesthetics with lipid bilayers investigated by 1H MAS NMR spectroscopy. *Biochim. Biophys. Acta* 1818:3010–3018.
9. Castro, V., B. Stevensson, . . ., and A. Maliniak. 2008. NMR investigations of interactions between anesthetics and lipid bilayers. *Biochim. Biophys. Acta* 1778:2604–2611.

5 Annexes

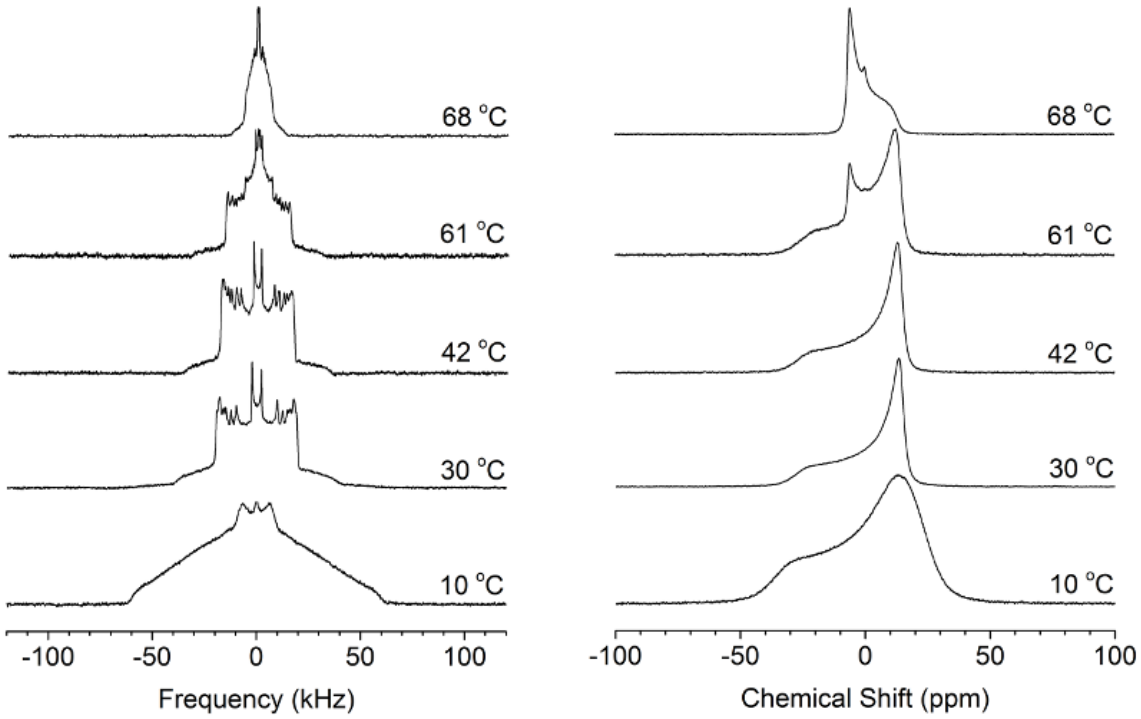

Fig. Anx 1: The ^{2}H (left column) and ^{31}P (right column) NMR spectra of POPE/CerC16-d_{31} 95/5 dispersion. The acquisition temperature is indicated on the right.

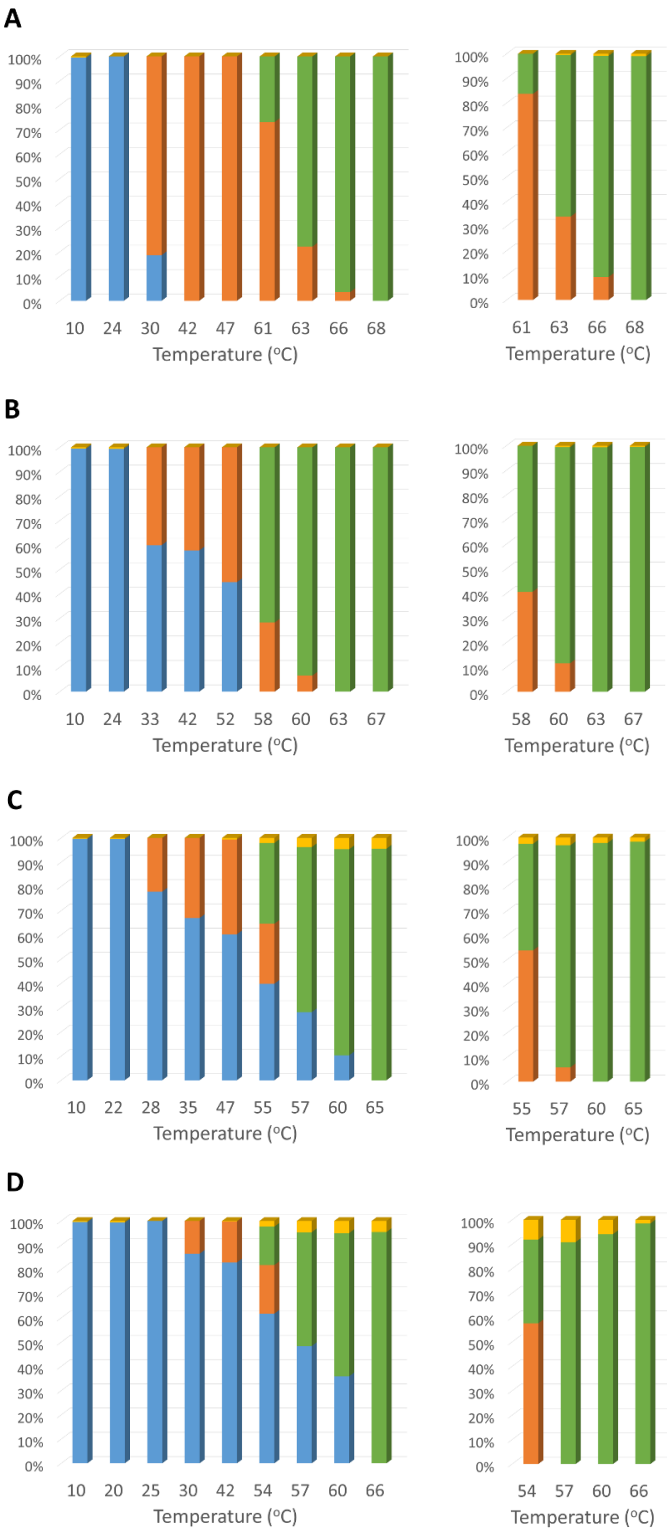

Fig. Anx 2: The phase distribution graphs derived from the ^{2}H- (left column) and ^{31}P- (right column) NMR spectra of POPE/CerC16-d_{31} mixtures with molar ratio of (A) 95/05, (B) 90/10, (C) 85/15, and (D) 80/20. Blue, orange, green, and yellow represent L_{β}, L_{α}, H_{II}, and isotropic phases, respectively.

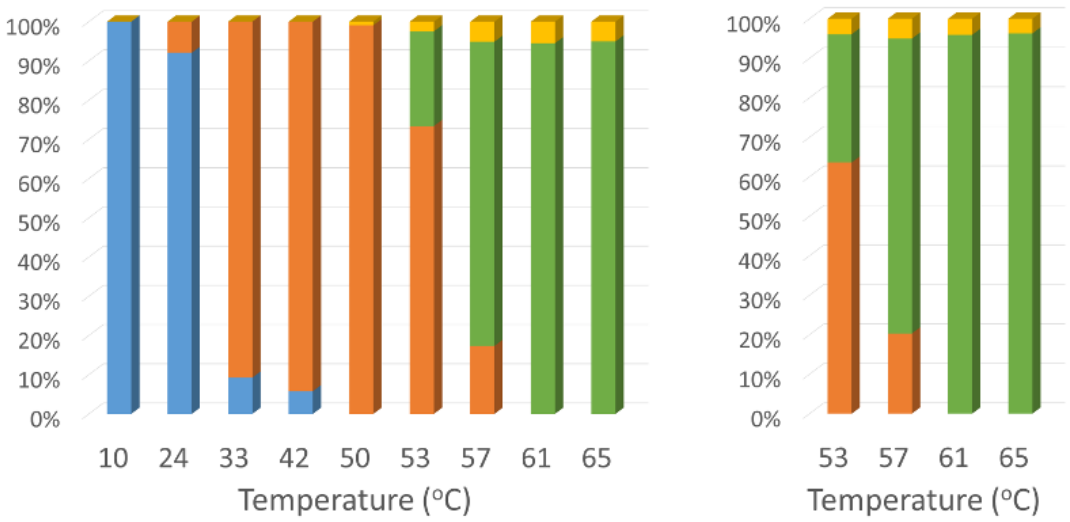

Fig. Anx 3: The ^{2}H (left) and ^{31}P (right) phase composition graphs of the POPE-d_{31}/CerC16 90/10 mixture. Blue, orange, green, and yellow represent L_{β}, L_{α}, H_{II}, and isotropic phases, respectively.

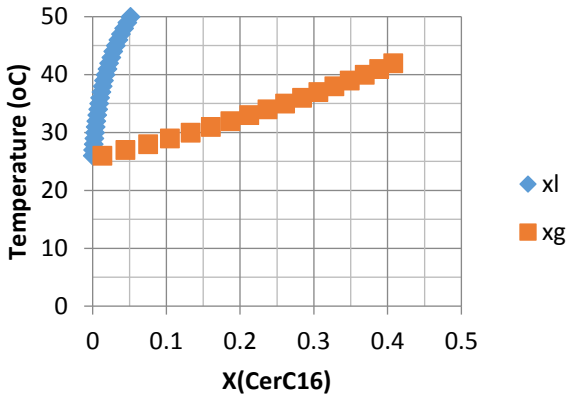

Fig. Anx 4: Theoretical phase diagram of the POPE/CerC16 system based on regular solution theory. ΔH (POPE) = 23.9 kJ/mol; T_m (POPE)= 25.6 °C (from our thermogram); ΔH (CerC16) = 57.7 kJ/mol; T_m (CerC16) = 90.0 °C (1).

1. Shah, J., J. M. Atienza, . . ., and G. G. Shipley. 1995. Structural and thermotropic properties of synthetic c16:0 (palmitoyl) ceramide: Effect of hydration. *J. Lipid Res.* 36:1936–1944.